The *Aquilegia* genome: adaptive radiation and an extraordinarily polymorphic chromosome with a unique history

Danièle Filiault[1], Evangeline S. Ballerini[2], Terezie Mandáková[3], Gökçe Aköz[1,4], Nathan Derieg[2], Jeremy Schmutz[5,6], Jerry Jenkins[5,6], Jane Grimwood[5,6], Shengqiang Shu[5], Richard D. Hayes[5], Uffe Hellsten[5], Kerrie Barry[5], Juying Yan[5], Sirma Mihaltcheva[5], Miroslava Karafiátová[7], Viktoria Nizhynska[1], Martin A. Lysak[3], Scott A. Hodges[2,*], Magnus Nordborg[1,*]

***For correspondence:**
scott.hodges@lifesci.ucsb.edu (SH); magnus.nordborg@gmi.oeaw.ac.at (MN)

[1]Gregor Mendel Institute, Austrian Academy of Sciences, Vienna BioCenter (VBC), Vienna, Austria; [2]Department of Ecology, Evolution, and Marine Biology, University of California Santa Barbara, Santa Barbara, USA; [3]Central-European Institute of Technology (CEITEC), Masaryk University, Brno, Czech Republic; [4]Vienna Graduate School of Population Genetics, Vienna, Austria; [5]Department of Energy Joint Genome Institute, Walnut Creek, California, USA; [6]HudsonAlpha Institute of Biotechnology, Huntsville, Alabama, USA; [7]Institute of Experimental Botany, Centre of the Region Haná for Biotechnological and Agricultural Research, Olomouc, Czech Republic

Abstract The columbine genus *Aquilegia* is a classic example of an adaptive radiation, involving a wide variety of pollinators and habitats. Here we present the genome assembly of *A. coerulea* 'Goldsmith', complemented by high-coverage sequencing data from 10 wild species covering the world-wide distribution. Our analyses reveal extensive allele sharing among species and demonstrate that introgression and selection played a role in the *Aquilegia* radiation. We also present the remarkable discovery that the evolutionary history of an entire chromosome differs from that of the rest of the genome – a phenomenon which we do not fully understand, but which highlights the need to consider chromosomes in an evolutionary context.

Introduction

Understanding adaptive radiation is a longstanding goal of evolutionary biology (***Schluter, 2000***). As a classic example of adaptive radiation, the *Aquilegia* genus has outstanding potential as a subject of such evolutionary studies (***Hodges et al., 2004***; ***Hodges and Derieg, 2009***; ***Kramer, 2009***). The genus is made up of about 70 species distributed across Asia, North America, and Europe (***Munz, 1946***) (**Figure 1**). Distributions of many *Aquilegia* species overlap or adjoin one another, sometimes forming notable hybrid zones (***Grant, 1952***; ***Hodges and Arnold, 1994b***; ***Li et al., 2014***). Additionally, species tend to be widely interfertile, especially within geographic regions (***Taylor, 1967***).

Phylogenetic studies have defined two concurrent, yet contrasting, adaptive radiations in *Aquilegia* (***Bastida et al., 2010***; ***Fior et al., 2013***). From a common ancestor in Asia, one radiation occurred in North America via Northeastern Asian precursors, while a separate Eurasian radiation took place

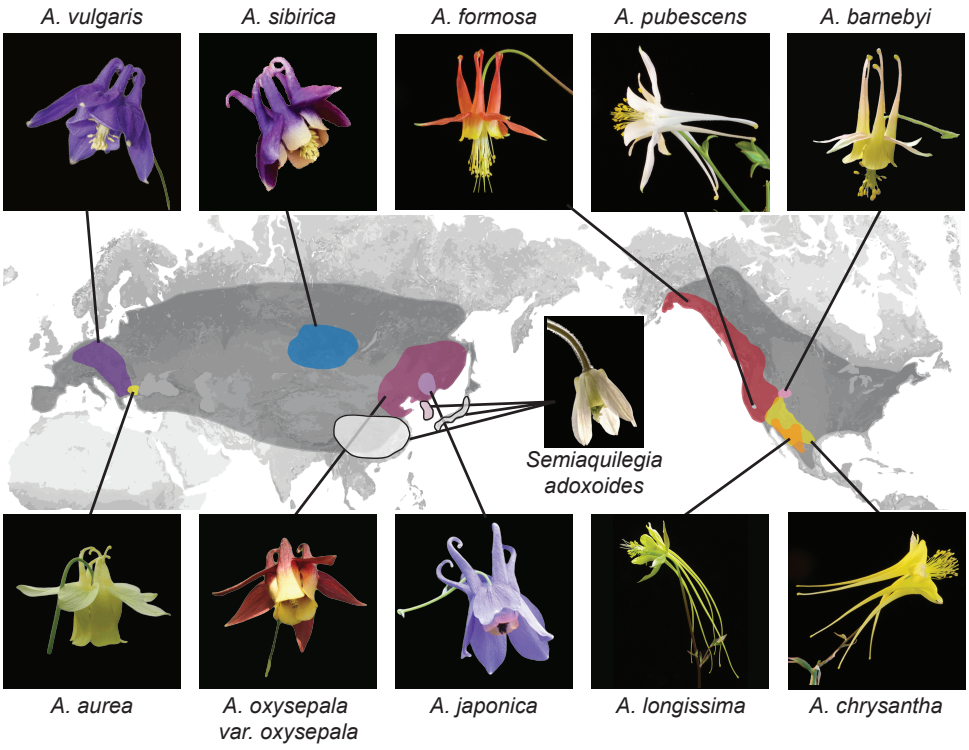

Figure 1. Distribution of *Aquilegia* species. There are ~70 species in the genus *Aquilegia*, broadly distributed across temperate regions of the Northern Hemisphere (grey). The 10 *Aquilegia* species sequenced here were chosen as representatives spanning this geographic distribution as well as the diversity in ecological habitat and pollinator-influenced floral morphology of the genus. *Semiaquilegia adoxoides*, generally thought to be the sister taxon to *Aquilegia* (***Fior et al., 2013***), was also sequenced. A representative photo of each species is shown and is linked to its approximate distribution.

in central and western Asia and Europe. While adaptation to different habitats is thought to be a common force driving both radiations, shifts in primary pollinators also play a substantial role in North America (***Whittall and Hodges, 2007***; ***Bastida et al., 2010***). Previous phylogenetic studies have frequently revealed polytomies (***Hodges and Arnold, 1994b***; ***Ro and Mcpheron, 1997***; ***Whittall and Hodges, 2007***; ***Bastida et al., 2010***; ***Fior et al., 2013***), suggesting that many *Aquilegia* species are very closely related.

Genomic data are beginning to uncover the extent to which interspecific variant sharing reflects a lack of strictly bifurcating species relationships, particularly in the case of adaptive radiation. Discordance between gene and species trees has been widely observed (***Novikova et al., 2016***) (and references 15,34-44 therein) (***Svardal et al., 2017***; ***Malinsky et al., 2017***), and while disagreement at the level of individual genes is expected under standard population genetics coalescent models (***Takahata, 1989***) (also known as "incomplete lineage sorting" (***Avise and Robinson, 2008***)), there is increased evidence for systematic discrepancies that can only be explained by some form of gene flow (***Green et al., 2010***; ***Novikova et al., 2016***; ***Svardal et al., 2017***; ***Malinsky et al., 2017***). The importance of admixture as a source of adaptive genetic variation has also become more evident (***Lamichhaney et al., 2015***; ***Mallet et al., 2016***; ***Pease et al., 2016***). Hence, rather than being a problem to overcome in phylogenetic analysis, non-bifurcating species relationships could actually describe evolutionary processes that are fundamental to understanding speciation itself. Here we generate an *Aquilegia* reference genome based on the horticultural cultivar *Aquilegia coerulea* 'Goldsmith' and perform resequencing and population genetic analysis of 10 additional

individuals representing North American, Asian, and European species, focusing in particular on the relationship between species.

Results

Genome assembly and annotation

We sequenced an inbred horticultural cultivar (*A. coerulea* 'Goldsmith') using a whole genome shotgun sequencing strategy. A total of 171,589 Sanger sequencing reads from seven genomic libraries (**Supplementary File 1**) were assembled to generate 2,529 scaffolds with an N50 of 3.1Mb (**Supplementary File 2**). With the aid of two genetic maps, we assembled these initial scaffolds into a 291.7 Mbp reference genome consisting of 7 chromosomes (282.6 Mbp) and an additional 1,027 unplaced scaffolds (9.13 Mbp) (Supplementary File 3). The completeness of the assembly was validated using 81,617 full length cDNAs from a variety of tissues and developmental stages (***Kramer and Hodges, 2010***), of which 98.69% mapped to the assembly. We also assessed assembly accuracy using Sanger sequencing of 23 full-length BAC clones. Of more than 3 million base pairs sequenced, only 1,831 were found to be discrepant between BAC clones and the assembled reference (**Supplementary File 4**). To annotate genes in the assembly, we used RNAseq data generated from a variety of tissues and *Aquilegia* species (**Supplementary File 5**), EST data sets (***Kramer and Hodges, 2010***), and protein homology support, yielding 30,023 loci and 13,527 alternate transcripts. The *A. coerulea* v3.1 genome release is available on Phytozome (https://phytozome.jgi.doe.gov/). For a detailed description of assembly and annotation, see **Materials and Methods**.

Polymorphism and divergence

We deeply resequenced one individual from each of ten *Aquilegia* species (**Figure 1 and Figure 1—figure supplement 1**). Sequences were aligned to the *A. coerulea* v3.1 reference using bwa-mem (***Li and Durbin, 2009***; ***Li, 2013***) and variants were called using GATK Haplotype Caller (***McKenna et al., 2010***). Genomic positions were conservatively filtered to identify the portion of the genome in which variants could be reliably called across all ten species (see **Materials and Methods** for alignment, SNP calling, and genome filtration details). The resulting callable portion of the genome was heavily biased towards genes and included 57% of annotated coding regions (48% of gene models), but only 21% of the reference genome as a whole.

Using these callable sites, we calculated nucleotide diversity as the percentage of pairwise sequence differences in each individual. Assuming random mating, this metric reflects both individual sample heterozygosity and nucleotide diversity in the species as a whole. Of the ten individuals, most had a nucleotide diversity of 0.2-0.35% (**Figure 2a**), similar to previous estimates of nucleotide diversity in *Aquilegia* (***Cooper et al., 2010***), yet lower than that of a typical outcrossing species (***Leffler et al., 2012***). While likely partially attributable to enrichment for highly conserved genomic regions with our stringent filtration, this atypically low nucleotide diversity could also reflect inbreeding. Additionally, four individuals in our panel had extended stretches of near-homozygosity (defined as nucleotide diversity < 0.1%) consistent with recent inbreeding (**Figure2-figure supplemental 1**). *Aquilegia* has no known self-incompatibility mechanism, and selfing does appear to be common. However, inbreeding in adult plants is generally low, suggesting substantial inbreeding depression (***Montalvo, 1994***; ***Herlihy and Eckert, 2002***; ***Yang and Hodges, 2010***).

We next considered nucleotide diversity between individuals as a measure of species divergence. Species divergence within a geographic region (0.38-0.86%) was often only slightly higher than within-species diversity, implying extensive variant sharing, while divergence between species from different geographic regions was markedly higher (0.81-0.97%; **Figure2a**). F_{ST} between geographic regions (0.245-0.271) was similar to that between outcrossing species of the *Arabidopsis* genus (***Novikova et al., 2016***), yet lower than between most vervet species pairs (***Svardal et al., 2017***), and higher than between cichlid groups in Malawi (***Loh et al., 2013***) or human ethnic groups (***McVean et al., 2012***). The topology of trees constructed with concatenated genome data (neighbor joining

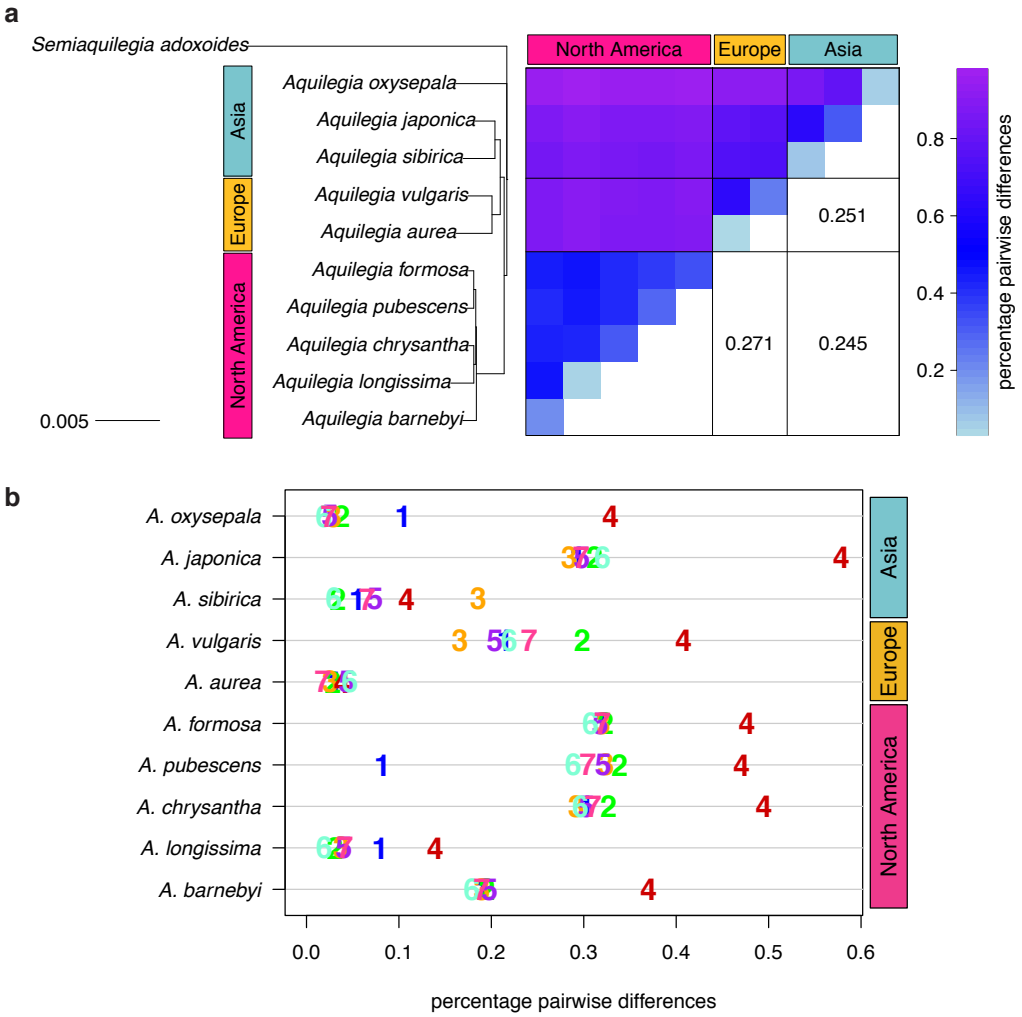

Figure 2. Polymorphism and divergence in *Aquilegia*. (a) The percentage of pairwise differences within each species (estimated from individual heterozygosity) and between species (divergence). F_{ST} values between geographic regions are given on the lower half of the pairwise differences heatmap. Both heatmap axes are ordered according to the neighbor joining tree to the left. This tree was constructed from a concatenated data set of reliably-called genomic positions. (b) Polymorphism within each sample by chromosome. Per chromosome values are indicated by the chromosome number.

(**Figure 2a**), RAxML (**Figure 2-figure supplemental 2a**)) were in broad agreement with previous *Aquilegia* phylogenies (***Hodges and Arnold, 1994a***; ***Ro and Mcpheron, 1997***; ***Whittall and Hodges, 2007***; ***Bastida et al., 2010***; ***Fior et al., 2013***), with one exception: while *A. oxysepala* is sister to all other *Aquilegia* species in our analysis, it had been placed within the large Eurasian clade with moderate to strong support in previous studies (***Bastida et al., 2010***; ***Fior et al., 2013***).

Surprisingly, levels of polymorphism were generally strikingly higher on chromosome four (**Figure 2b**). Exceptions were apparently due to inbreeding, especially in the case of the *A. aurea* individual, which appears to be almost completely homozygous (**Figure 2a** and **Figure 2-figure supplemental 1**). The increased polymorphism on chromosome four is only partly reflected in increased divergence to an outgroup species (*Semiaquilegia adoxoides*), suggesting that it represents deeper coalescence times rather than simply a higher mutation rate (mean ratio chromosome four/genome at fourfold degenerate sites: polymorphism=2.258, divergence=1.201, **Supplementary File 6**).

Discordance between gene and species trees

To assess discordance between gene and species (genome) trees, we constructed a cloudogram of trees drawn from 100kb windows across the genome (**Figure 3a**). Fewer than 1% of these window-based trees were topologically identical to the species tree. North American species were consistently separated from all others (96% of window trees) and European species were also clearly delineated (67% of window trees). However, three bifurcations delineating Asian species were much less common: the *A. japonica* and *A. sibirica* sister relationship (45% of window trees), *A. oxysepala* as sister to all other species (30% of window trees), and the split demarcating the Eurasian radiation (31% of window trees). These results demonstrate a marked discordance of gene and species trees throughout both *Aquilegia* radiations.

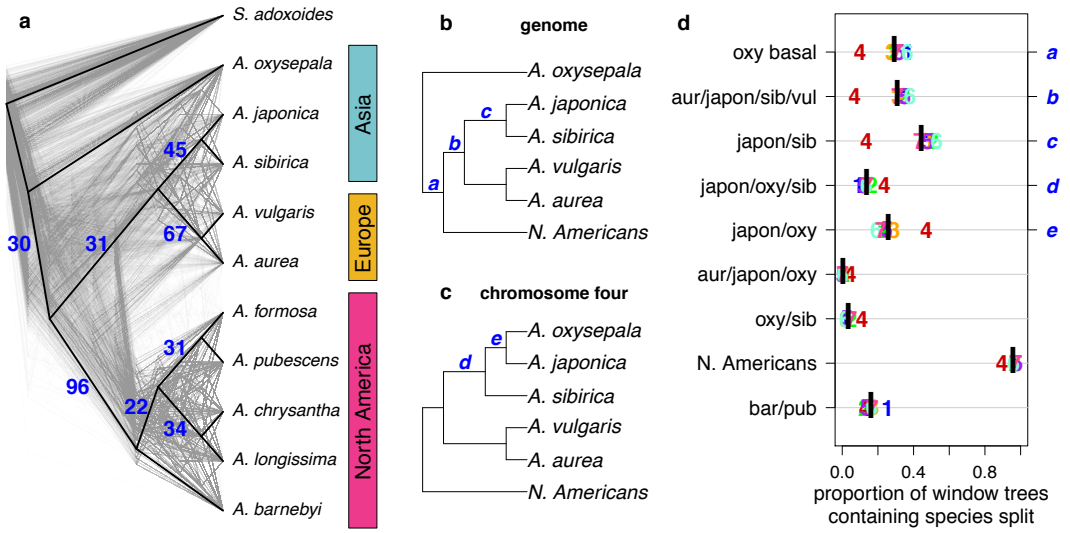

Figure 3. Discordance between gene and species trees. (a) Cloudogram of neighbor joining (NJ) trees constructed in 100kb windows across the genome. The topology of each window-based tree is co-plotted in grey and the whole genome NJ tree shown in **Figure 2a** is superimposed in black. Blue numbers indicate the percentage of window trees that contain each of the subtrees observed in the whole genome tree. (b) Genome NJ tree topology. Blue letters a-c on the tree denote subtrees a-c in panel (d). (c) Chromosome four NJ tree topology. Blue letters d and e on the tree denote subtrees d and e in panel (d). (d) Prevalence of each subtree that varied significantly by chromosome. Genomic (black bar) and per chromosome (chromosome number) values are given.

The gene tree analysis also highlighted the unique evolutionary history of chromosome four. Of 217 unique subtrees observed in gene trees, nine varied significantly in frequency between chromosomes (chi-square test *p*-value < 0.05 after Bonferroni correction; **Figure 3b-d** and **Figure 3-figure supplementals 1 and 2**). Trees describing a sister species relationship between *A. pubescens* and *A. barnebyi* were more common on chromosome one, but chromosome four stood out with respect to eight other relationships, most of them related to *A. oxysepala* (**Figure 3d**). Although *A. oxysepala* was sister to all other species in our genome tree, the topology of the chromosome four tree was consistent with previously-published phylogenies in that it placed *A. oxysepala* within the Eurasian clade (***Bastida et al., 2010***; ***Fior et al., 2013***)(**Figure 2-figure supplemental 2b,c**). Subtree prevalences were in accordance with this topological variation (**Figure 3b-d**). The subtree delineating all North American species was also less frequent on chromosome four, indicating that the history of the chromosome is discordant in both radiations. We detected no patterns in the prevalence of any chromosome-discordant subtree that would suggest structural variation or a large introgression (**Figure 3-figure supplemental 3**).

Polymorphism sharing across the genus

We next polarized variants against an outgroup species (*S. adoxoides*) to explore the prevalence and depth of polymorphism sharing. Private derived variants accounted for only 21-25% of polymorphic sites in North American species and 36-47% of variants in Eurasian species (**Figure 4a**). The depth of polymorphism sharing reflected the two geographically-distinct radiations. North American species shared 34-38% of their derived variants within North America, while variants in European and Asian species were commonly shared across two geographic regions (18-22% of polymorphisms, predominantly shared between Europe and Asia; **Figure 4b,c**; **Figure 4-figure supplemental 1**). Strikingly, a large percentage of derived variants occurred in all three geographic regions (22-32% of polymorphisms, **Figure 4d**), demonstrating that polymorphism sharing in *Aquilegia* is extensive and deep.

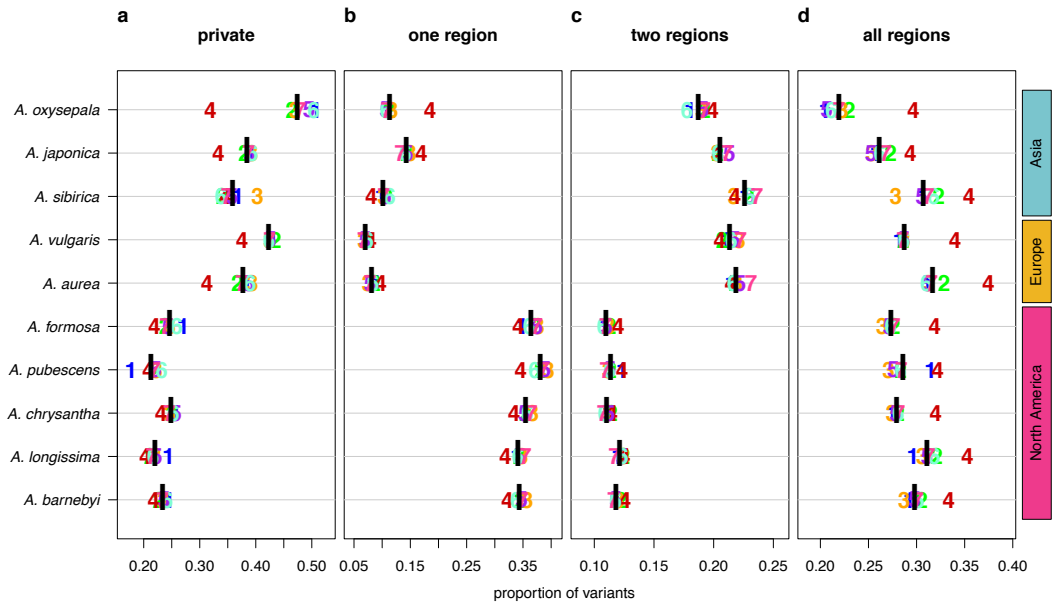

Figure 4. Sharing patterns of derived polymorphisms. Proportion of derived variants (a) private to an individual species, (b) shared within the geography of origin, (c) shared across two geographic regions, and (d) shared across all three geographic regions. Genomic (black bar) and chromosome (chromosome number) values, for all 10 species.

In all species examined, the proportion of deeply shared variants was higher on chromosome four (**Figure 4d**), largely due to a reduction in private variants, although sharing at other depths was also reduced in some species. Variant sharing on chromosome four within Asia was higher in both *A. oxysepala* and *A. japonica* (Figure 4b), primarily reflecting higher variant sharing between these species (**Figure 6a**).

Evidence of gene flow

Consider three species, H1, H2, and H3. If H1 and H2 are sister species relative to H3, then, in the absence of gene flow, H3 must be equally related to H1 and H2. The D statistic (***Green et al., 2010***; ***Durand et al., 2011***) tests this hypothesis by comparing the number of derived variants shared between H3, and H1 and H2, respectively. A non-zero D statistic reflects an asymmetric pattern of allele sharing, implying gene flow between H3 and one of the two sister species, i.e., that speciation was not accompanied by complete reproductive isolation. If *Aquilegia* diversification occurred via a series of bifurcating species splits characterized by reproductive isolation, bifurcations in the species tree should represent combinations of sister and outgroup species with symmetric allele sharing patterns (D=0). Given the high discordance of gene and species trees at the individual

species level, we focused on testing a simplified tree topology based on the three groups whose bifurcation order seemed clear: (1) North American species, (2) European species, and (3) Asian species not including *A. oxysepala*. In all tests, *S. adoxoides* was used to determine the ancestral state of alleles.

We first tested each North American species as H3 against all combinations of European and Asian (without *A. oxysepala*) species as H1 and H2 (**Figure 5a-c**). As predicted, the North American split was closest to resembling speciation with strict reproductive isolation, with little asymmetry in allele sharing between North American and Asian species and low, but significant, asymmetry between North American and European species (**Figure 5b**). Next, we considered allele sharing between European and Asian (without *A. oxysepala*) species (**Figure 5 d,e**). Here we found non-zero D-statistics for all species combinations. Interestingly, the patterns of asymmetry between these two regions were reticulate: Asian species shared more variants with the European *A. vulgaris* while European species shared more derived alleles with the Asian *A. sibirica*. D statistics therefore demonstrate widespread asymmetry in variant sharing between *Aquilegia* species, suggesting that speciation processes throughout the genus were not characterized by strict reproductive isolation.

Although non-zero D statistics are usually interpreted as being due to gene flow in the form of admixture between species, they can also result from gene flow between incipient species. Either way, speciation precedes reproductive isolation. The possibility that different levels of purifying selection in H1 or H2 explain the observed D statistics can probably be ruled out, since D statistics do not differ when calculated with only fourfold degenerate sites (p-value < 2.2×10^{-16}, adjusted R^2=0.9942, **Figure 5-source data 1**). Non-zero D statistics could also indicate that the bifurcation order tested was incorrect, but even tests based on alternative tree topologies resulted in few D statistics that equal zero (**Figure 5-source data 1**). Therefore, the non-zero D statistics observed in *Aquilegia* most likely reflect a pattern of reticulate evolution throughout the genus.

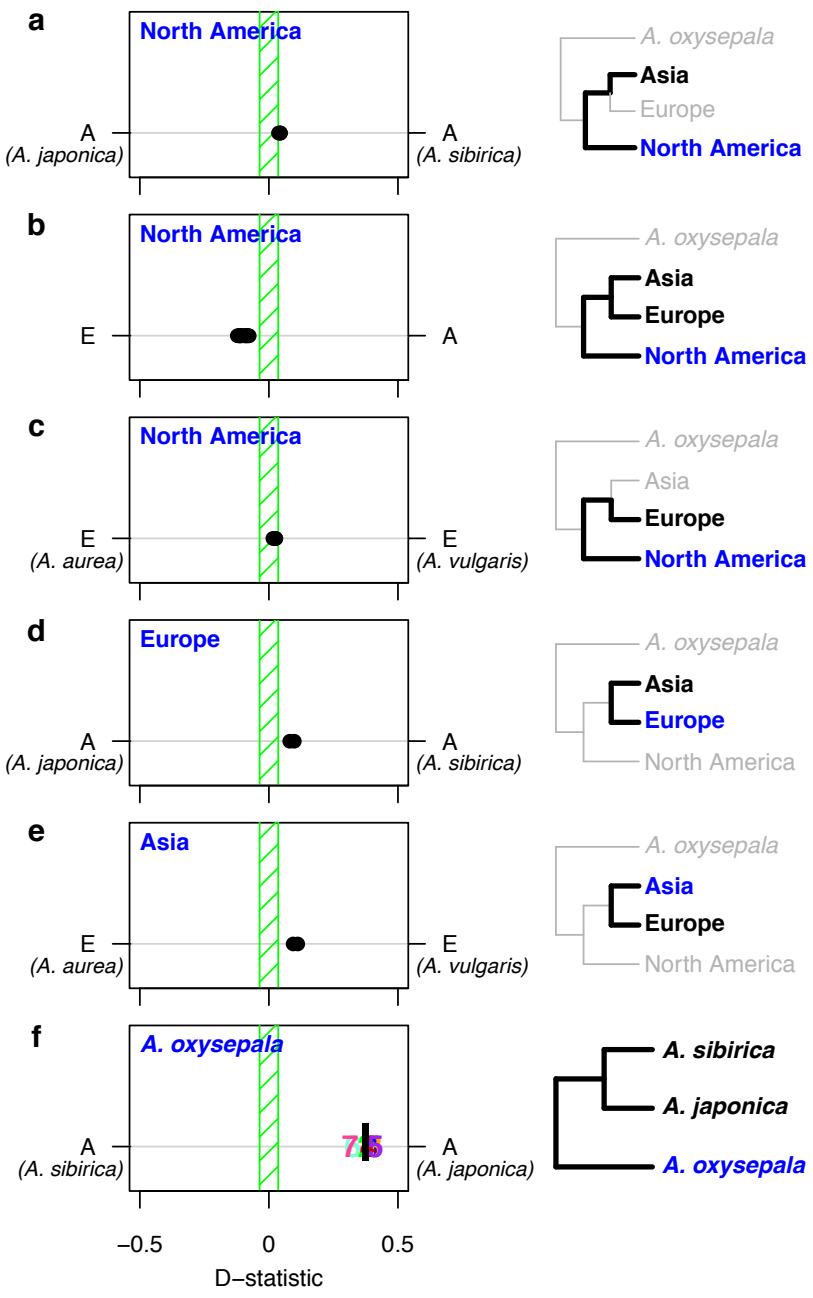

Figure 5. D statistics demonstrate gene flow during *Aquilegia* speciation. D statistics for tests with (a-c) all North American species, (d) both European species, (e) Asian species other than *A. oxysepala*, and (f) *A. oxysepala* as H3 species. All tests use *S. adoxoides* as the outgroup. D statistics outside the green shaded areas are significantly different from zero. In (a-e), each individual dot represents the D statistic for a test done with a unique species combination. In (f), D statistics are presented by chromosome (chromosome number) or by the genome-wide value (black bar). In all panels, E=European and A=Asian without *A. oxysepala*. In some cases, individual species names are given when the geographical region designation consists of a single species. Right hand panels are a graphical representation of the D statistic tests in the corresponding left hand panels. Trees are a simplified version of the genome tree topology (**Figure 2b**), in which the bold subtree(s) represent the bifurcation considered in each set of tests. H3 species are noted in blue while the H1 and H2 species are specified in black. (**Figure 5-source data 1**)

Since variant sharing between *A. oxysepala* and *A. japonica* was higher on chromosome four (**Figure 6a**), and hybridization between these species has been reported (***Li et al., 2014***) we wondered whether gene flow could explain the discordant placement of *A. oxysepala* between chromosome four and genome trees (**Figure 3b,c**). Indeed, when the genome tree was taken as the bifurcation order, D statistics were elevated between these species (**Figure 5f**). A relatively simple coalescent model allowing for bidirectional gene flow between *A. oxysepala* and *A. japonica* (**Figure 6b**) demonstrated that doubling the population size (N) to reflect chromosome four's polymorphism level (i.e. halving the coalescence rate) could indeed shift tree topology proportions (**Figure 6c**, row 2). However, recreating the observed allele sharing ratios on chromosome four (**Figure 6a**) required some combination of increased migration (m) and/or N (**Figure 6c**, rows 3-4). It is plausible that gene flow might differentially affect chromosome four, and we will return to this topic in the next section. Although the similarity of the D statistic across chromosomes (**Figure 5f**) might seem inconsistent with increased migration on chromosome four, the D statistic reaches a plateau in our simulations such that many different combinations of m and N produce similar D values (**Figure 6c** and **Figure 6-figure supplemental 1**). Therefore, an increase in migration rate and deeper coalescence can explain the tree topology of chromosome four, a result that might explain inconsistencies in *A. oxysepala* placement in previous phylogenetic studies (***Bastida et al., 2010***; ***Fior et al., 2013***).

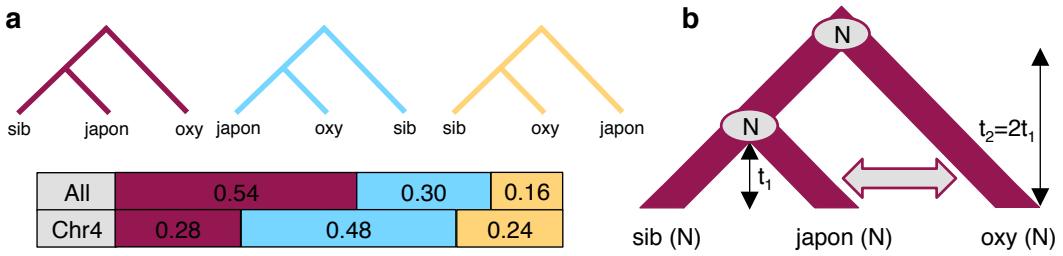

c

m	N	Simulated tree topology proportions			D-stat
$2x10^{-5}$	11667	0.53	0.31	0.14	0.38
$2x10^{-5}$	23334	0.41	0.41	0.17	0.44
$4x10^{-5}$	23334	0.30	0.49	0.20	0.42
$2x10^{-5}$	46668	0.30	0.49	0.20	0.42

Figure 6. The effect of differences in coalescence time and gene flow on tree topologies. (a) The observed proportion of informative derived variants supporting each possible Asian tree topology genome-wide and on chromosome four. Species considered include *A. oxysepala* (oxy), *A. japonica* (japon), and *A. sibirica* (sib). (b) The coalescent model with bidirectional gene flow in which *A. oxysepala* diverges first at time t2, but later hybridizes with *A. japonica* between t=0 and t1 at a rate determined by per-generation migration rate, m. The population size (N) remains constant at all times. (c) The proportion of each tree topology and estimated D statistic for simulations using four combinations of m and N values (t1=1 in units of N generations). The combination presented in the first row (m=$2x10^{-5}$ and N=11667) generates tree topology proportions that match observed allele sharing proportions genomewide. Simulations with increased m and/or N (rows 3-4) result in proportions which more closely resemble those observed for chromosome four. Colors in proportion plots refer to tree topologies in (a), with black bars representing the residual probability of seeing no coalescence event. While this simulation assumes symmetric gene flow, similar results were seen for models incorporating both unidirectional and asymmetric gene flow (**Figure 6-figure supplementals 1 and 2**).

The pattern of polymorphism on chromosome four

In most of the sequenced *Aquilegia* species, the level of polymorphism on chromosome four is twice as high as in the rest of the genome (**Figure 2b**). This unique pattern could be: 1) an artifact of biases in polymorphism detection between chromosomes, 2) the result of a higher neutral mutation rate on chromosome four, or 3) the result of deeper coalescence times on chromosome four (allowing more time for polymorphism to accumulate).

While it is impossible to completely rule out phenomena such as cryptic copy number variants (CNV), for the pattern to be entirely attributable to artefacts would require that half of the polymorphism on chromosome four be spurious. This scenario is extremely unlikely given the robustness of the result to a variety of CNV detection methods (**Supplementary File 7**). Similarly, the pattern cannot wholly be explained by a higher neutral mutation rate. If this were the case, both divergence and polymorphism would be elevated to the same extent on chromosome four (***Kimura, 1983***). As noted above, this not the case (**Supplementary File 6**). Thus the higher level of polymorphism on chromosome four must to some extent reflect differences in coalescence time, which can only be due to selection.

Although it is clear that selection can have a dramatic effect on the history of a single locus, the chromosome-wide pattern we observe (**Figure 2-figure supplemental 1**) is difficult to explain. Chromosome four recombines freely (**Figure 7a**), suggesting that polymorphism is not due to selection on a limited number of linked loci, such as might be observed if driven by an inversion or large supergene. Selection must thus be acting on a very large number of loci across the chromosome.

Balancing selection is known to elevate polymorphism, and in a number of plant species, disease resistance (*R*) genes show signatures of balancing selection (***Karasov et al., 2014***). While such signatures have not yet been demonstrated in *Aquilegia*, chromosome four is enriched for the defense gene GO category, which encompasses *R* genes (**Table 1**). However, while significant, this enrichment involves a relatively small number of genes (less than 2% of genes on chromosome four) and is therefore unlikely to completely explain the polymorphism pattern (***Nordborg and Innan, 2003***).

Another potential explanation is reduced purifying selection. In fact, several characteristics of chromosome four suggest that it could experience less purifying selection than the rest of the genome. Gene density is markedly lower (**Table 2 and Figure 7b**), it harbors a higher proportion of repetitive sites (**Table 2**), and is enriched for many transposon families, including Copia and Gypsy elements (**Supplementary File 8**). Additionally, a higher proportion of genes on chromosome four were either not expressed or expressed at a low level (**Figure 7-figure supplemental 2**). Gene models on the chromosome were also more likely to contain variants that could disrupt protein function (**Table 2**). Taken together, these observations suggest less purifying selection on chromosome four.

Reduced purifying selection could also explain the putatively higher gene flow between *A. oxysepala* and *A. japonica* on chromosome four (**Figure 6**); the chromosome would be more permeable to gene flow if loci involved in the adaptive radiation were preferentially located on other chromosomes. Indeed, focusing on *A. oxysepala/A. japonica* gene flow, we found a negative relationship between introgression and gene density in the *Aquilegia* genome (**Figure 7c**, *p*-value=2.202×10^{-7}, adjusted R-squared=0.068), as would be expected if purifying selection limited introgression. Notably, this relationship is the same for chromosome four and the rest of the genome (*p*-value=0.051), suggesting that gene flow on chromosome four is higher simply because the gene density is lower.

However, the picture is very different for nucleotide diversity. While there is a negative relationship between gene density and neutral nucleotide diversity genome-wide (*p*-value=5.174×10^{-6}, adjusted R-squared=0.052), more careful analysis reveals that chromosome four has a completely different distribution from the rest of the genome (**Figure 7d**, *p*-value$<2 \times 10^{-16}$). In both cases, there is a weak (statistically insignificant) negative relationship between gene density and nucleotide diver-

Table 1. GO term enrichment on chromosome four

GO	Corrected *P*-value	Number on Chr_04 Observed	Number on Chr_04 Expected	Percent of Chr_04 genes	GO term
0043531	5.61×10^{-79}	140	9	7.57	ADP binding
0016705	4.40×10^{-48}	179	39	9.68	Oxidoreductase activity, acting on paired donors, with incorporation or reduction of molecular oxygen
0004497	7.19×10^{-46}	158	32	8.55	Monooxygenase activity
0005506	2.73×10^{-41}	181	46	9.79	Iron ion binding
0020037	2.57×10^{-37}	186	53	10.06	Heme binding
0010333	1.72×10^{-15}	39	4	2.11	Terpene synthase activity
0016829	2.08×10^{-13}	39	5	2.11	Lyase activity
0055114	9.53×10^{-10}	247	149	13.36	Oxidation-reduction process
0016747	6.66×10^{-5}	44	16	2.38	Transferase activity, transferring acyl groups other than amino-acyl groups
0000287	1.23×10^{-4}	42	15	2.27	Magnesium ion binding
0008152	2.56×10^{-4}	137	83	7.41	Metabolic process
0006952	3.60×10^{-4}	32	10	1.73	Defense response
0004674	4.52×10^{-4}	23	5	1.24	Protein serine/threonine kinase activity
0016758	1.35×10^{-3}	44	18	2.38	Transferase activity, transferring hexosyl groups
0005622	4.14×10^{-3}	14	42	0.76	Intracellular
0008146	2.68×10^{-2}	9	1	0.49	Sulfotransferase activity
0016760	3.72×10^{-2}	12	2	0.65	Cellulose synthase (UDP-forming) activity

sity (chromsome four:*p*-value=0.0814, adjusted R-squared=0.0303, rest of the genome:*p*-value=0.315, adjusted R-squared=3.373×10^{-5}), but nucleotide diversity is consistently much higher for chromosome four. Thus the genome-wide relationship reflects this systematic difference between chromosome four and the rest of the genome, and gene density differences alone are insufficient to explain higher polymorphism on chromosome four. Therefore, if reduced background selection explains higher polymorphism on this chromosome, something other than gene density must distinguish it from the rest of the genome. As noted above, there is reason to believe that purifying selection, in general, is lower on this chromosome.

For comparison with data from other organisms, we performed the partial correlation analysis of ***Corbett-Detig et al.*** (***2015***). Here we found a significant relationship between neutral diversity and recombination rate (without chromosome four, Kendall's tau=0.222, *p*-value=3.804×10^{-6}), putting *Aquilegia* on the higher end of estimates of the strength of linked selection in herbaceous plants.

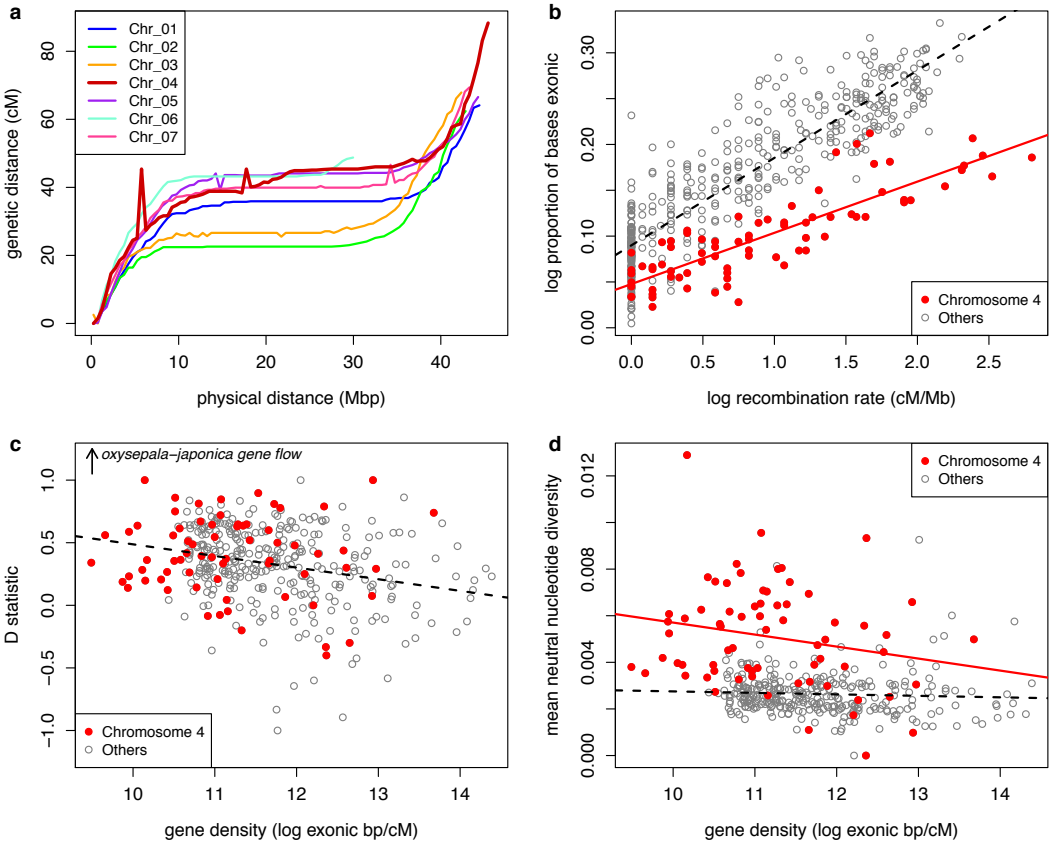

Figure 7. Recombination and selection on chromosome four (a) Physical vs. genetic distance for all chromosomes calculated in an *A. formosa* x *A. pubescens* mapping population. High nucleotide diversity on chromosome four was also observed in parental plants of this population (**Figure 7-supplemental 1**. (b) Relationship between gene density (proportion exonic) and recombination rate (main effect *p*-value$<2 \times 10^{-16}$, chromsome four effect *p*-value$<2 \times 10^{-16}$, interaction *p*-value$<1.936 \times 10^{-11}$, adjusted R-squared=0.8045). (c) Relationship between gene density and D statistic for *A. oxysepala* and *A. japonica* gene flow. (d) Relationship between gene density and mean neutral nucleotide diversity. **Figure 7-source data 1**

Table 2. Content of the *A. coerulea* v3.1 reference by chromosome

	Chromosome							
	1	2	3	4	5	6	7	Genome
Number of genes	5041	4390	4449	3149	4786	3292	4443	29550
Genes per Mb	112	102	104	69	107	108	102	100
Mean gene length (bp)	3629	3641	3689	3020	3712	3620	3708	3580
Percent repetitive	38.9	41.1	39.1	54.2	39.4	39.3	40.6	42.0
Percent genes with HIGH effect variant	25.3	23.8	23.6	32.3	24.1	22.1	23.6	24.7
Percent GC	36.8	37.0	36.9	37.0	37.1	36.8	36.8	37.0

While selection during the *Aquilegia* radiation contributes to the pattern of polymorphism on chromosome four, the pattern itself predates the radiation. Divergence between *Aquilegia* and *Semiaquilegia* is higher on chromosome four (2.77% on chromosome four, 2.48% genome-wide, **Table 3**), as is nucleotide diversity within *Semiaquilegia* (0.16% chromosome four, 0.08% genome-wide, **Table 3**). This suggests that the variant evolutionary history of chromosome four began before the *Aquilegia*/*Semiaquilegia* split.

Table 3. Population genetics parameters for *Semiaquilegia* by chromosome

	Percent pairwise differences							
	Chromosome							
	1	2	3	4	5	6	7	Genome
Polymorphism within *Semiaquilegia*	0.079	0.085	0.081	0.162	0.076	0.078	0.071	0.082
Divergence between *Aquilegia* and *Semiaquilegia*	2.46	2.47	2.47	2.77	2.48	2.47	2.47	2.48

The 35S and 5S rDNA loci are uniquely localized to chromosome four

The observation that one *Aquilegia* chromosome is different from the others is not novel; previous cytological work described a single nucleolar chromosome that appeared to be highly heterochromatic (***Linnert, 1961***). Using fluorescence in situ hybridization (FISH) with rDNA and chromosome four-specific bulked oligo probes (***Han et al., 2015***), we confirmed that both the 35S and 5S rDNA loci were localized uniquely to chromosome four in two *Aquilegia* species and *S. adoxoides* (**Figure 8**). The chromosome contained a single large 35S repeat cluster proximal to the centromeric region in all three species. Interestingly, the 35S locus in *A. formosa* was larger than that of the other two species and formed variable bubbles and fold-backs on extended pachytene chromosomes similar to structures previously observed in *Aquilegia* hybrids (***Linnert, 1961***) (**Figure 8**, last panels). The 5S rDNA locus was also proximal to the centromere on chromosome four, although slight differences in the number and position of the 5S repeats between species highlight the dynamic nature of this gene cluster. However, no chromosome appeared to be more heterochromatic than others in our analyses (**Figure 8**); FISH with 5-methylcytosine antibody showed no evidence for hypermethylation on chromosome four (**Figure 8-figure supplemental 1**) and GC content was similar for all chromosomes (**Table 2**). However, similarities in chromosome four organization across all three species reinforce the idea that the exceptionality of this chromosome predated the *Aquilegia*/*Semiaquilegia* split and raise the possibility that rDNA clusters could have played a role in the variant evolutionary history of chromosome four.

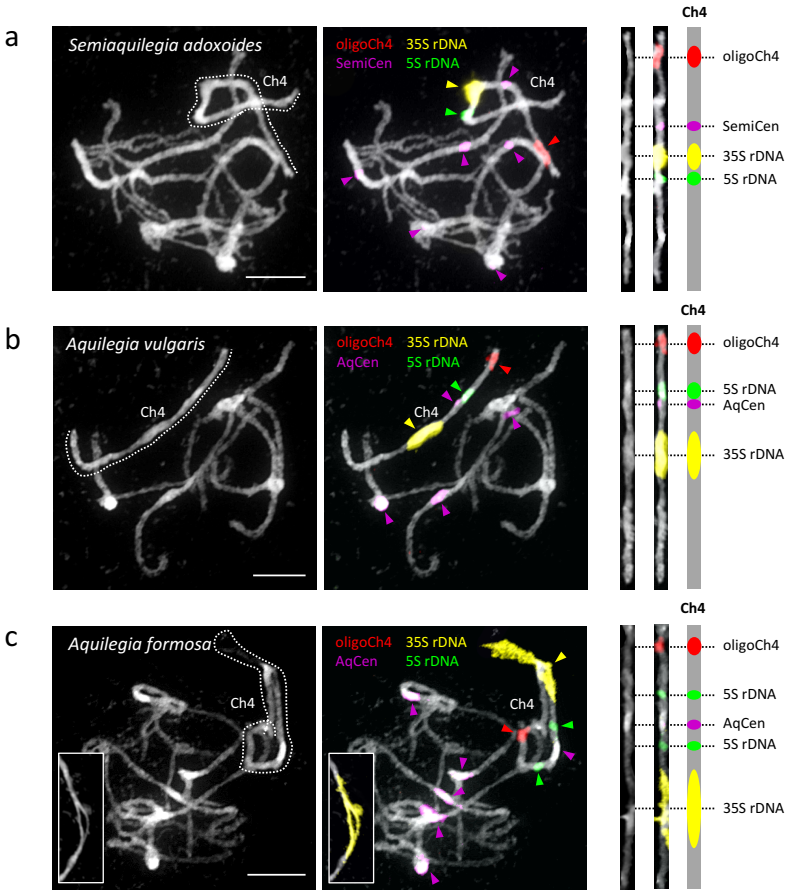

Figure 8. Cytogenetic characterization of chromosome four in *Semiaquilegia* and *Aquilegia* species. Pachytene chromosome spreads were probed with probes corresponding to oligoCh4 (red), 35S rDNA (yellow), 5S rDNA (green) and two (peri)centromeric tandem repeats (pink). Chromosomes were counterstained with DAPI. Scale bars = 10 µm.

Discussion

We constructed a reference genome for the horticultural cultivar *Aquilegia coerulea* 'Goldsmith' and resequenced ten *Aquilegia* species with the goal of understanding the genomics of ecological speciation in this rapidly diversifying lineage. Although our reference genome size is smaller than previous estimates (~300Mb versus ~500Mb, (***Bennett et al., 1982***; ***Bennett and Leitch, 2011***)), the completeness and accuracy of our assembly (**Supplementary File 4**), as well as consistency between reference and *k*-mer based estimates of genome size (**Supplementary File 9**), suggest that this difference is likely due to highly repetitive content, including the large rDNA loci on chromosome four.

Variant sharing across the *Aquilegia* genus is widespread and deep, even across exceptionally large geographical distances. Although much of this sharing is presumably due to stochastic processes, as expected given the rapid time-scale of speciation, asymmetry of allele sharing demonstrates that the process of speciation has been reticulate throughout the genus, and that gene flow has been a common feature. *Aquilegia* species diversity therefore appears to be an example of ecological speciation, rather than being driven by the development of intrinsic barriers to gene flow (***Coyne et al., 2004***; ***Schluter and Conte, 2009***; ***Seehausen et al., 2014***). In the future, studies incorporating more taxa and/or population-level variation will provide additional insight into the dynamics of this process. Given the extent of variant sharing, it will be also be interesting to explore the role of standing variation and admixture in adaptation throughout the genus.

Our analysis also led to the remarkable discovery that the evolutionary history of an entire chromosome differed from that of the rest of the genome. The average level of polymorphism on chromosome four is roughly twice that of the rest of the genome and gene trees on this chromosome appear to reflect a different species relationship (**Figure 3**). To the best of our knowledge, with the possible exception of sex chromosomes (***Toups and Hahn, 2010***; ***Nam et al., 2015***), such chromosome-wide patterns have never been observed before (although recombination has been shown to affect hybridization; see ***Schumer et al., 2017***). Importantly, this chromosome is large and appears to be freely recombining, implying that these differences are unlikely to be due to a single evolutionary event, but rather reflect the accumulated effects of evolutionary forces acting differentially on the chromosome.

While no single explanation for the elevated polymorphism on chromosome four has emerged, selection clearly plays a role. Our results demonstrate that chromosome four could affected by balancing selection as well as by reduced purifying and/or background selection. Future work will focus on clarifying the role and importance of each of these types of selection, and determining whether the rapid adaptive radiation in *Aquilegia* has played a role in accelerating the differences between chromosome four and the rest of the genome.

The chromosome four patterns, appear to predate the *Aquilegia* adaptive radiation, however, extending at least into the genus *Semiaquilegia*. Differences in gene content may thus be a proximal explanation for the higher polymorphism levels on chromosome four, but we still lack an explanation for why these differences would have been established on chromosome four in the first place. One possibility is that chromosome four is a reverted sex chromosome, a phenomenon that has been observed in *Drosophila* (***Vicoso and Bachtrog, 2013***). Although species with separate sexes exist in the Ranunculaceae, these transitions seem to be recent (***Soza et al., 2012***), and all *Aquilegia* and *Semiaquilegia* species are hermaphroditic. Furthermore, no heteromorphic sex chromosomes have been observed in the Ranunculales (***Westergaard, 1958***; ***Ming et al., 2011***), making this an unlikely hypothesis. It has also been suggested that chromosome four is a fusion of two homeologous chromosomes (***Linnert, 1961***), as could result from the ancestral whole genome duplication (***Cui et al., 2006***; ***Vanneste et al., 2014***; ***Tiley et al., 2016***), however, analysis of synteny blocks shows that this is not the case (***Aköz and Nordborg, 2018***).

B chromosomes also have evolutionary histories that differ from those of other chromosomes. Like chromosome four, B chromosomes accumulate repetitive sequences and frequently contain

rDNA loci (***Jones, 1995***; ***Green, 1990***; ***Valente et al., 2017***). However, chromosome four does not appear to be supernumerary, and unlike B chromosomes which seem to have only a few loci, chromosome four contains thousands of coding sequences (**Table 2**). Again, while it is impossible to rule out the hypothesis that chromosome four has been impacted by the reincorporation of B chromosomes into the A genome, this would be a novel phenomenon.

It is tempting to speculate that the distinct evolutionary history of chromosome four is connected to its large rDNA repeat clusters. Although rDNA clusters in *Aquilegia* and *Semiaquilegia* are consistently found on chromosome four, cytology demonstrates that the exact location of these loci is dynamic. Could the movement of these components somehow contribute to an accumulation of structural variants, copy number variants, and repeats that make chromosome four an inhospitable and unreliable place to harbor critical coding sequences? If so, then forces of genome evolution could underlie the more proximal causes (lower gene content and reduced selection) of decreased polymorphism on chromosome four.

rDNA clusters could also have played a role in initiating chromosome four's different evolutionary history. Cytological (***Langlet, 1927***, ***1932***) and phylogenetic (***Ro et al., 1997***; ***Wang et al., 2009***; ***Cossard et al., 2016***) work separates the Ranunculaceae into two main subfamilies marked by different base chromosome numbers: the Thalictroideae (T-type, base n=7, including *Aquilegia* and *Semiaquilegia*) and the Ranunculoideae (R-type, predominantly base n=8). In the three T-type species tested here, the 35S is proximal to the centromere, a localization seen for only 3.5% of 35S sites reported in higher plants (***Roa and Guerra, 2012***). In contrast, all R-type species examined have terminal or subterminal 45S loci (***Hizume et al., 2013***; ***Mlinarec et al., 2006***; ***Weiss-Schneeweiss et al., 2007***; ***Liao et al., 2008***). Given that 35S repeats can be fragile sites (***Huang et al., 2008***) and 35S rDNA clusters and rearrangement breakpoints co-localize (***Cazaux et al., 2011***), a 35S-mediated chromosomal break could explain differences in base chromosome number between R-type and T-type species. If the variant history of chromosome four can be linked to this this R- vs T-type split, this could implicate chromosome evolution as the initiator of chromosome four's variant history. Comparative genomics work within the Ranunculaceae will therefore be useful for understanding the role that rDNA repeats have played in chromosome evolution and could provide additional insight into how rDNA could have contributed to chromosome four's variant evolutionary history.

In conclusion, the *Aquilegia* genus is a beautiful example of adaptive radiation through ecological speciation. Although our current genome analyses based on a limited number of individuals and species, we see evidence that the radiation was shaped by introgression, selection, and the presence of abundant standing variation. Ongoing work focuses on understanding the contributions of each of these factors to adaptation in *Aquilegia* using population and quantitative genetics. Additionally, the unexpected variant evolutionary history of chromosome four, while still a mystery, illustrates that standard population genetics models are not always sufficient to the explain the pattern of variation across the genome. Future studies of chromosome four have the potential to increase our understanding of how genome evolution, chromosome evolution, and population genetics interact to generate organismal diversity.

Materials and Methods

Genome sequencing, assembly, and annotation

Sequencing

Sequencing was performed on *Aquilegia coerulea* cv 'Goldsmith', an inbred line constructed and provided by Todd Perkins of Goldsmith Seeds (now part of Syngenta). The line was of hybrid origin of multiple taxa and varieties of Aquilegia and then inbred. The sequencing reads were collected with standard Sanger sequencing protocols at the Department of Energy Joint Genome Institute in Walnut Creek, California and the HudsonAlpha Institute for Biotechnology. Libraries included two 2.5 Kb libraries (3.36x), two 6.5 Kb libraries (3.70x), two 33Kb insert size fosmid libraries (0.36x), and one 124kb insert size BAC library (0.17x). The final read set consists of 171,859 reads for a total of

3.411 Gb high quality bases (**Supplementary File 1**).

Genome assembly and construction of pseudomolecule chromosomes

A total of 171,589 sequence reads (7.59x assembled sequence coverage) were assembled using our modified version of Arachne v.20071016 (***Jaffe et al., 2003***) with parameters maxcliq1=120 n_haplotypes=2 max_bad_look=2000 START=SquashOverlaps BINGE_AND_PURGE_2HAP=True.

This produced 2,529 scaffolds (10,316 contigs), with a scaffold N50 of 3.1 Mb, 168 scaffolds larger than 100 kb, and total genome size of 298.6 Mb (**Supplementary File 2**). Two genetic maps (*A. coerulea* 'Goldsmith' x *A. chrysantha* and *A. formosa* x *A. pubescens*) were used to identify 98 misjoins in the initial assembly. Misjoins were identified by a linkage group/syntenic discontinuity coincident with an area of low BAC/fosmid coverage. A total of 286 scaffolds were ordered and oriented with 279 joins to form 7 chromosomes. Each chromosome join is padded with 10,000 Ns. The remaining scaffolds were screened against bacterial proteins, organelle sequences, GenBank nr and removed if found to be a contaminant. Additional scaffolds were removed if they (a) consisted of >95% 24mers that occurred 4 other times in scaffolds larger than 50kb (957 scaffolds, 6.7 Mb), (b) contained only unanchored RNA sequences (14 scaffolds, 651.9 Kb), or (c) were less than 1kb in length (303 scaffolds). Significant telomeric sequence was identified using the TTTAGGG repeat, and care was taken to make sure that it was properly oriented in the production assembly. The final release assembly (*A. coerulea* 'Goldsmith' v3.0) contains 1,034 scaffolds (7,930 contigs) that cover 291.7 Mb of the genome with a contig N50 of 110.9 kb and a scaffold L50 of 43.6 Mb (**Supplementary File 3**.

Validation of genome assembly

Completeness of the euchromatic portion of the genome assembly was assessed using 81,617 full length cDNAs (***Kramer and Hodges, 2010***). The aim of this analysis is to obtain a measure of completeness of the assembly, rather than a comprehensive examination of gene space. The cDNAs were aligned to the assembly using BLAT (***Kent, 2002***) (Parameters: -t=dna –q=rna –extendThroughN -noHead) and alignments >=90% base pair identity and >=85% EST coverage were retained. The screened alignments indicate that 79,626 (98.69%) of the full length cDNAs aligned to the assembly. The cDNAs that failed to align were checked against the NCBI nucleotide repository (nr), and a large fraction were found to be arthropods (*Acyrthosiphon pisum*) and prokaryotes (*Acidovorax*).

A set of 23 BAC clones were sequenced in order to assess the accuracy of the assembly. Minor variants were detected in the comparison of the fosmid clones and the assembly. In all 23 BAC clones, the alignments were of high quality (< 0.35% bp error), with an overall bp error rate (including marked gap bases) in the BAC clones of 0.24% (1,831 discrepant bp out of 3,063,805; **Supplementary File 4**).

Genomic repeat and transposable element prediction

Consensus repeat families were predicted de novo for the *A. coerulea* v3.0 assembly by the RepeatModeler pipeline (***Smit and Hubley, 2008-2015***). These consensus sequences were annotated for PFAM and Panther domains, and any sequences known to be associated with non-TE function were removed. The final curated library was used to generate a softmasked version of the *A. coerulea* v3.0 assembly.

Transcript assembly and gene model annotation

A total of 246 million paired-end and a combined 1 billion single-end RNAseq reads from a diverse set of tissues and related *Aquilegia* species (**Supplementary File 5**) were assembled using PERTRAN (***Shu et al., 2013***) to generate a candidate set containing 188,971 putative transcript assemblies. The PERTRAN candidate set was combined with 115,000 full length ESTs (the 85,000 sequence cDNA library derived from an *A. formosa X A. pubescens* cross (***Kramer and Hodges, 2010***) and 30,000 Sanger sequences of *A. formosa* sequenced at JGI) and aligned against the v3.0 assembly of the *A. coerulea* genome by PASA (***Haas et al., 2003***).

Loci were determined by BLAT alignments of above transcript assemblies and/or BLASTX of the proteomes of a diverse set of Angiosperms (*Arabidopsis thaliana* TAIR10, *Oryza sativa* v7, *Glycine max* Wm82.a2.v1, *Mimulus guttatus* v2, *Vitus vinifera* Genoscape.12X and *Poplar trichocarpa* v3.0). These protein homology seeds were further extended by the EXONERATE algorithm. Gene models were predicted by homology-based predictors, FGENESH+ (***Salamov and Solovyev, 2000***), FGENESH_EST (similar to FGENESH+, but using EST sequence to model splice sites and introns instead of putative translated sequence), and GenomeScan (***Yeh et al., 2001***).

The final gene set was selected from all predictions at a given locus based on evidence for EST support or protein homology support according to several metrics, including Cscore, a protein BLASTP score ratio to homology seed mutual best hit (MBH) BLASTP score, and protein coverage, counted as the highest percentage of protein model aligned to the best of its Angiosperm homologs. A gene model was selected if its Cscore was at least 0.40 combined with protein homology coverage of at least 45%, or if the model had EST coverage of at least 50%. The predicted gene set was also filtered to remove gene models overlapping more than 20% with a masked Repeatmodeler consensus repeat region of the genome assembly, except for such cases that met more stringent score and coverage thresholds of 0.80 and 70% respectively. A final round of filtering to remove putative transposable elements was conducted using known TE PFAM and Panther domain homology present in more than 30% of the length of a given gene model. Finally, the selected gene models were improved by a second round of the PASA algorithm, which potentially included correction to selected intron splice sites, addition of UTR, and modeling of alternative spliceforms.

The resulting annotation and the *A. coerulea* 'Goldsmith' v3.0 assembly make up the *A. coerulea* v3.1 genome release, available on Phytozome (https://phytozome.jgi.doe.gov/)

Sequencing of species individuals

Sequencing, mapping and variant calling

Individuals of 10 *Aquilegia* species and *Semiaquilegia adoxoides* were resequenced (**Figure 1** and **Figure1-figure supplement 1**). One sample (*A. pubescens*) was sequenced at the Vienna Biocenter Core Facilities Next Generation Sequencing (NGS) unit in Vienna, Austria and the others were sequenced at the JGI (Walnut Creek, CA, USA). All libraries were prepared using standard/slightly modified Illumina protocols and sequenced using paired-end Illumina sequencing. *Aquilegia* species read length was 100bp, the *S. adoxoides* read length was 150bp, and samples were sequenced to a depth of 58-124x coverage (**Supplementary File 10**). Sequences were aligned against *A. coerulea* v3.1 with bwa mem (bwa mem -t 8 -p -M)(***Li and Durbin, 2009***; ***Li, 2013***). Duplicates and unmapped reads were removed with SAMtools (***Li et al., 2009***). Picardtools (***Pic, 2018***) was used to clean the resulting bam files (CleanSam.jar), to remove duplicates (MarkDuplicates.jar), and to fix mate pair problems (FixMateInformation.jar). GATK 3.4 (***McKenna et al., 2010***; ***DePristo et al., 2011***) was used to identify problem intervals and do local realignments (RealignTargetCreator and IndelRealigner). The GATK Haplotype Caller was used to generate gVCF files for each sample. Individual gVCF files were merged and GenotypeGVCFs in GATK was used to call variants.

Variant filtration

Variants were filtered to identify positions in the single-copy genome that could be reliable called across all *Aquilegia* individuals. Variant Filtration in GATK 3.4 (***McKenna et al., 2010***; ***DePristo et al., 2011***) was used to filter multialleleic sites, indels +/-10bp, sites identified with Repeatmasker (***Smit et al., 2013-2015***), and sites in previously-determined repetitive elements (see "***Genomic repeat and transposable element prediction***" *above*). We required a minimum coverage of 15 in all samples and a genotype call (either variant or non-variant) in all accessions. Sites with less than 0.5x log median coverage or greater than -0.5x log median coverage in any sample were also removed. A table of the number of sites removed by each filter is in **Supplementary File 11**.

Polarization

S. adoxoides was added to the *Aquilegia* individual species data set and the above filtration was repeated (**Supplementary File 12**). The resulting variants were then polarized against *S. adoxoides*, resulting in nearly 1.5 million polarizable variant positions. A similar number of derived variants was detected in all species (**Supplementary File 13**), suggesting no reference bias resulting from the largely North American provenance of the *A. coerulea* v3.1 reference sequence used for mapping.

Evolutionary analysis

Basic population genetics

Basic population genetics parameters including nucleotide diversity (polymorphism and divergence) and F_{ST} were calculated using custom scripts in R (***R Core Team, 2014***). Nucleotide diversity was calculated as the percentage of pairwise differences in the mappable part of the genome. F_{ST} was calculated as in ***Hudson et al.*** (***1992***). To identify fourfold degenerate sites, four pseudo-vcfs replacing all positions with A,T,C, or G, respectively, were used as input into SNPeff (***Cingolani et al., 2012***) to assess the effect of each pseudo-variant in reference to the *A. coerulea* v3.1 annotation. Results from all four output files were compared to identify genic sites that caused no predicted protein changes.

Tree and cloudogram construction

Trees were constructed using a concatenated data set of all nonfiltered sites, either genome-wide or by chromosome. Neighbor joining (NJ) trees were made using the ape (***Paradis et al., 2004***) and phangorn (***Schliep, 2011***) packages in R (***R Core Team, 2014***) using a Hamming distance matrix and the nj command. RAxML trees were constructed using the default settings in RAxML (***Stamatakis, 2014***). All trees were bootstrapped 100 times. The cloudogram was made by constructing NJ trees using concatenated nonfiltered SNPs in non-overlapping 100kb windows across the genome (minimum of 100 variant positions per window, 2,387 trees total) and plotted using the densiTree package in phangorn (***Schliep, 2011***).

Differences in subtree frequency by chromosome

For each of the 217 subtrees that had been observed in the cloudogram, we calculated the proportion of window trees on each chromosome containing the subtree of interest and performed a test of equal proportions (prop.test in R (***R Core Team, 2014***)) to determine whether the prevalence of the subtree varied by chromosome. For significantly-varying subtrees, we then performed another test of equal proportions (prop.test in R (***R Core Team, 2014***)) to ask whether subtree proportion on each chromosome was different from the genome-wide proportion. The appropriate Bonferroni multiple testing correction was applied to *p*-values obtained in both tests (n=217 and n=70, respectively).

Tests of D-statistics

D-statistics tests were performed in ANGSD (***Korneliussen et al., 2014***) using non-filtered sites only. ANGSD ABBABABA was run with a block size of 100000 and results were bootstrapped. Tests were repeated using only fourfold degenerate sites.

Modelling effects of migration rate and effective population size

Using the markovchain (***Spedicato, 2017***) package in R (***R Core Team, 2014***), we simulated a simple coalescent model with the assumptions as follows: (1) population size is constant (N alleles) at all times, (2) *A. oxysepala* split from the population ancestral to *A. sibirica* and *A. japonica* at generation t_2=2*t, (3) *A. sibirica* and *A. japonica* split from each other at generation t_1=t, and (4) there was gene flow between *A. oxysepala* and *A. japonica* between t=0 and t_1. A first Markov Chain simulated migration with symmetric gene flow (m_1=m_2) and coalescence between t=0 and t_1 (*Five-State Markov Chain*, **Supplementary File 14**). This process was run for T (t*N) generations to get the starting

probabilities for the second process, which simulated coalescence between t_1 and t_2+1 (*Eight-State Markov Chain*, **Supplementary File 15**). The second process was run for N generations. After first identifying a combination of parameters that minimized the difference between simulated versus observed gene genealogy proportions, we then reran the process with increased migration rate and/or N to check if simulated proportions matched observed chromosome four-specific proportions. We also ran the initial chain under two additional models of gene flow: unidirectional (m_2=0) and asymmetric (m_1=2*m_2).

Robustness of chromosome four patterns to filtration

Variant filtration as outlined above was repeated with a stringent coverage filter (keeping only positions with +/-0.15x log median coverage in all samples) and nucleotide diversity per chromosome was recalculated. Nucleotide diversity per chromosome was also recalculated after removal of copy number variants detected by the readDepth package (***Miller et al., 2011***) in R (***R Core Team, 2014***), after the removal of tandem duplicates as determined by running DAGchainer (***Haas et al., 2004***) on *A. coerulea* v3.1 in CoGe SynMap (***Lyons and Freeling, 2008***), as well as after the removal of heterozygous variants for which both alleles were not supported by an equivalent number of reads (a log read number ratio <-0.3 or >0.3).

Construction of an *A. formosa* x *A. pubescens* genetic map

Mapping and variant detection

Construction of the *A. formosa* x *A. pubescens* F2 cross was previously described in ***Hodges et al.*** (***2002***). One *A. pubescens* F0 line (pub.2) and one *A. formosa* F0 line (form.2) had been sequenced as part of the species resequencing explained above. Libraries for the other *A. formosa* F0 (form.1) were constructed using a modified Illumina Nextera library preparation protocol (***Baym et al., 2015***) and sequenced at at the Vincent J. Coates Genomics Sequencing Laboratory (UC Berkeley). Libraries for the other *A. pubescens* F0 (pub.1), and for both F1 individuals (F1.1 and F1.2), were prepared using a slightly modified Illumina Genomic DNA Sample preparation protocol (***Rabanal et al., 2017***) and sequenced at the Vienna Biocenter Core Facilities Next generation sequencing (NGS) unit in Vienna, Austria. All individual libraries were sequenced as 100 bp paired-end reads on the Illumina HiSeq platform to 50-200x coverage. A subset of F2s were sequenced at the Vienna Biocenter Core Facilities Next Generation Sequencing (NGS) unit in Vienna, Austria (70 lines). Libraries for the remaining F2s (246 lines) were prepared and sequenced by the JGI (Walnut Creek, CA). All F2s were prepared using the Illumina multiplexing protocol and sequenced on the Illumina HiSeq platform to generate 100 bp paired end reads. Samples were 96-multiplexed to generate about 1-2x coverage. Sequences for all samples were aligned to the *A. coerulea* 'Goldsmith' v3.1 reference genome using bwa mem with default parameters (***Li and Durbin, 2009***; ***Li, 2013***). SAMtools 0.1.19 (***Li et al., 2009***) mpileup (-q 60 -C 50 -B) was used to call variable sites in the F1 individuals. Variants were filtered for minimum base quality and minimum and maximum read depth (-Q 30, -d20, -D150) using SAMtools varFilter. Variable sites that had a genotype quality of 99 in the F1s were genotyped in F0 plants to generate a set of diagnostic alleles for each parent of origin. To assess nucleotide diversity, F0 and F1 samples were additionally processed with the mapping and variant calling pipeline as described for species samples above.

Genotyping of F2s, genetic map construction, and recombination rate estimation

F2s were genotyped in genomic bins of 0.5 Mb in regions of moderate to high recombination and 1 Mb in regions with very low or no recombination, as estimated by the *A. coerulea* 'Goldsmith' x *A. chrysantha* cross used to assemble the *A. coerulea* 'Goldsmith' v3.1 reference genome (see "**Genome assembly and construction of pseudomolecule chromosomes**"). Ancestry of each bin was independently determined for each of the four parents. The ratio of:

$$\frac{\text{reads containing a diagnostic allele}}{\text{reads potentially containing a diagnostic allele}}$$

was calculated for each parent in each bin. If this ratio was between 0.4 and 0.6, the bin was assigned to the parent containing the diagnostic allele. Bins with ratios between 0.1 and 0.4 were considered more closely to determine whether they represented a recombination event or discordance between the physical map of *A. formosa*/*A. pubescens* and the *A. coerulea* 'Goldsmith' v3.1 reference genome. If a particular bin had intermediate frequencies for many F2 individuals, indicative of a map discordance, bin margins were adjusted to capture the discordant fragment and allow it to independently map during genetic map construction.

Bin genotypes were used as markers to assemble a genetic map using R/qtl v.1.35-3 (***Broman et al., 2003***). Genetic maps were initially constructed for each chromosome of a homolog pair in the F2s. After the two F1 homologous chromosome maps were estimated, data from each chromosome was combined to estimate the combined genetic map. Several bins in which genotypes could not accurately be determined either due to poor read coverage, lack of diagnostic SNPs, or unclear discordance with the reference genome were dropped from further recombination rate analysis.

To measure recombination in each F1 parent, genetic maps were initially constructed for each chromosome of a homolog pair in the F2s. After the two F1 homologous chromosome maps were estimated, data from each chromosome was combined to estimate the combined genetic map. In order to calculate the recombination rate for each bin, a custom R script (***R Core Team, 2014***) was written to count the number of recombination events in the bin which was then averaged by the number of haploid genomes assessed (n=648). To calculate cM per Mb, this number was multiplied by 100 and divided by the bin size in Mb.

Chromosome four gene content and background selection

Unless noted, all analyses were done in R(***R Core Team, 2014***).

Gene content, repeat content, and variant effects

Gene density and mean gene length were calculated considering primary transcripts only. Percent repetitive sequence was determined from annotation. The effects of variants was determined with SNPeff (***Cingolani et al., 2012***) using the filtered variant data set and primary transcripts.

Repeat family content

The RepeatClassifier utility from RepeatMasker (***Smit et al., 2013-2015***) was used to assign *A . coerulea* v3.1 repeats to known repetitive element classes. For each of the 38 repeat families identified, the insertion rate per Mb was calculated for each chromosome and a permutation test was performed to determine whether this proportion was significantly different on chromosome four versus genome-wide. Briefly, we ran 1000 simulations to determine the number of insertions expected on chromosome four if insertions occurred randomly at the genome-wide insertion rate and then compared this distribution with the observed copy number in our data.

GO term enrichment

A two-sided Fisher's exact test was performed for each GO term to test whether the term made up a more extreme proportion on of genes on chromosome four versus the proportion in the rest of the genome. *P*-values were Bonferroni corrected for the number of GO terms (n=1936).

Quantification of gene expression

We sequenced whole transcriptomes of sepals from 21 species of *Aquilegia* (**Supplementary File 5**). Tissue was collected at the onset of anthesis and immediately immersed in RNAlater (Ambion) or snap frozen in liquid nitrogen. Total RNA was isolated using RNeasy kits (Qiagen) and mRNA was separated using poly-A pulldown (Illumina). Obtaining amounts of mRNA sufficient for preparation of sequencing libraries required pooling multiple sepals together into a single sample; we used tissue from a single individual when available, but often had to pool sepals from separate individuals into a single sample. We prepared sequencing libraries according to manufacturer's protocols

except that some libraries were prepared using half-volume reactions (Illumina RNA-sequencing for *A. coerulea*, and half-volume Illumina TruSeq RNA for all other species). Libraries for *A. coerulea* were sequenced one sample per lane on an Illumina GAII (University of California, Davis Genome Center). Libraries for all other species were sequenced on an Illumina HiSeq at the Vincent J. Coates Genomics Sequencing Laboratory (UC Berkeley), with samples multiplexed using TruSeq indexed adapters (Illumina). Reads were aligned to *A. coerulea 'Goldsmith' v3.1* using bwa aln and bwa samse (***Li and Durbin, 2009***). We processed alignments with SAMtools (***Li et al., 2009***) and custom scripts were used to count the number of sequence reads per transcript for each sample. Reads that aligned ambiguously were probabilistically assigned to a single transcript. Read counts were normalized using calcNormFactors and cpm functions in the R package edgeR (***Robinson et al., 2010***; ***McCarthy et al., 2012***). Mean abundance was calculated for each transcript by first averaging samples within a species, and then averaging across all species.

Relationships between recombination, gene density, introgression, and neutral nucleotide diversity

Recombination rates were taken from the *A. formosa* x *A. pubescens* analysis described in **Construction of an *A. formosa* x *A. pubescens* genetic map**. We calculated neutral nucleotide diversity, proportion exonic, and the D statistic for each genomic bin used in constructing the genetic map. Polymorphism at fourfold degenerate sites was calculated per species/individual, and the mean of all 10 species was taken. The number of exonic bases was determined using primary gene models from the *A. coerulea* v3.1 annotation and both proportion exonic bases and gene density (exonic bases/cM) were calculated. To obtain window D statistics, we parsed the ANGSD raw output file (*out.abbababa) generated for the test of *A. oxysepala* as the outgroup and *A. japonica* and *A. sibirica* as sister species (described in **Tests of D-statistics**).

We performed linear models in R (***R Core Team, 2014***), log transforming as appropriate, to look at the relationship between (1) exonic proportion and recombination rate, (2) D statistic and gene density (exonic base pairs per cM), and (3) neutral nucleotide diversity and gene density. For each relationship, we tested two models: one considering the genome as a whole and a second that tested for differences between chromosome four and the rest of the genome, including an interaction term when significant. If the second model showed a significant *p*-value difference for chromosome four, we also performed individual linear models for both chromosome four and the rest of the genome.

We also calculated the partial correlation coefficient between recombination rate and neutral nucleotide diversity accounting for gene density as in (***Corbett-Detig et al., 2015***).

Genome size determination

Genome size was assessed using the *k*-mer counting method. Histograms of 20-base-pair *k*-mer counts were generated in Jellyfish 2.2.6 (***Marçais and Kingsford, 2011***) using the fastq files of all 10 resequenced *Aquilegia* species. Using these histograms, estimates of genome size and repetitive proportion were made using the findGSE library (***Sun et al., 2018***) in R (***R Core Team, 2014***).

Cytology

Chromosome preparation

Inflorescences of the analyzed accessions were fixed in ethanol:acetic acid (3:1) overnight and stored in 70% ethanol at -20°C. Selected flower buds were rinsed in distilled water and citrate buffer (10 mM sodium citrate, pH 4.8; 2 × 5 min) and incubated in an enzyme mix (0.3% cellulase, cytohelicase, and pectolyase; all Sigma-Aldrich) in citrate buffer at 37°C for 3 to 6 h. Individual anthers were disintegrated on a microscope slide in a drop of citrate buffer and 15 to 30 µl of 60% acetic acid. The suspension was spread on a hot plate at 50°C for 0.5 to 2 min. Chromosomes were fixed by adding 100 µl of ethanol:acetic acid (3:1). The slide was dried with a hair dryer, postfixed in 4% formaldehyde dissolved in distilled water for 10 min, and air-dried. Chromosome preparations

were treated with 100 µg/ml RNase in 2× sodium saline citrate (SSC; 20× SSC: 3 M sodium chloride, 300 mM trisodium citrate, pH 7.0) for 60 min and with 0.1 mg/ml pepsin in 0.01 M HCl at 37°C for 2 to 5 min; then postfixed in 4% formaldehyde in 2× SSC, and dehydrated in an ethanol series (70%, 90%, and 100%, 2 min each).

Probe preparation from oligo library

An oligonucleotide library consisting of 20,628 oligonucleotide probes to the 2 Mb region spanning the positions 42-44 Mbp of chromosome four (oligoCh4) was designed and synthesized by MYcroarray (Ann Arbor, MI). This library was used to prepare the chromosome four-specific painting probe (***Han et al., 2015***). Briefly, oligonucleotides were multiplied in two independent amplification steps. First, 0.2 ng DNA from the immortal library was amplified from originally ligated adaptors in emulsion PCR using primers provided by MYcroarray together with the library. Emulsion PCR was used to increase the representativeness of amplified products (***Murgha et al., 2014***). Droplets were generated manually by stirring of oil phase at 1000 × g at 4°C for 10 min and then the aqueous phase was added. 500 ng of amplified product was used as a template for T7 in vitro transcription with MEGAshortscript T7 Kit (Invitrogen) – the second amplification step. RNA was purified on RNeasy spin columns (Qiagen) and labeled in reverse transcription with biotin-labeled R primer. The product – RNA:DNA hybrid – was washed using Zymo Quick-RNA MiniPrep (Zymo Research), hydrolysed by RNase and obtained DNA was cleaned again with Zymo Kit to get the final single-stranded DNA probe.

Fluorescence in situ hybridization (FISH)

Species resequencing data was used to determing the (peri)centromeric satellite repeats of *Semiaquilegia* (SemiCen) and *Aquilegia* (AqCen) (***Melters et al., 2013***); the detected AqCen sequence corresponds to the previously-described centromeric repeat (***Melters et al., 2013***). Bulked oligonucleotides specific for chromosome four (oligoCh4), (peri)centromeric satellite repeats, *Arabidopsis thaliana* BAC clone T15P10 (AF167571) containing 35S rRNA genes, and *A. thaliana* clone pCT4.2 (M65137) corresponding to a 500-bp 5S rRNA repeat were used as probes. All DNA probes were labeled with biotin-dUTP, digoxigenin-dUTP or Cy3-dUTP by nick translation (***Mandáková et al., 2016***). Selected labeled DNA probes were pooled together, ethanol precipitated, dissolved in 20 µl of 50% formamide, 10% dextran sulfate in 2× SSC and pipetted onto microscope slides. The slides were heated at 80°C for 2 min and incubated at 37°C overnight. Posthybridization washing was performed in 20% formamide in 2× SSC at 42°C (2 × 5 min). Hybridized probes were visualized through fluorescently labeled antibodies against biotin or digoxigenin (***Mandáková et al., 2016***). Chromosomes were counterstained with 4',6-diamidino-2-phenylindole (DAPI, 2 µg/ml) in Vectashield antifade. Fluorescence signals were analyzed and photographed using a Zeiss Axioimager epifluorescence microscope and a CoolCube camera (MetaSystems). Individual images were merged and processed using Photoshop CS software (Adobe Systems). Pachytene chromosomes in Figure 8 were straightened using the "straighten-curved-objects" plugin in the Image J software (***Kocsis et al., 1991***).

5-methylcytosine (5mC) immunodetection

For immunodetection of 5mC, chromosome spreads were prepared according to the procedure described above. Denaturation mixture containing 20 µl of 50% formamide, 10% dextran sulfate in 2× SSC was pipetted onto each microscope slide. The slides were heated at 80°C for 2 min, washed in 2× SSC (2 × 5 min) and incubated in bovine serum albumin solution (5% BSA, 0.2% Tween-20 in 4× SSC) at 37°C for 30 min. Immunodetection was performed using 100 µl of primary antibody against 5mC (mouse anti 5mC, Diagenode, diluted 1 : 100) at 37°C for 30 min. After washing in 2× SSC (2 × 5 min) the slides were incubated with the secondary antibody (Alexa Fluor 488 goat anti-mouse IgG, Invitrogen, diluted 1 : 200) at 37°C for 30 min, followed by washing in 2× SSC (2 × 5 min) and a dehydration in an ethanol series (70%, 90%, and 100%, 2 min each). Chromosomes were

counterstained with DAPI, fluorescence signals analyzed and photographed as described above. The slides were washed in 2× SSC (2 × 5 min), dehydrated in an ethanol series (70%, 90%, and 100%, 2 min each), and rehybridized with 35S rDNA probe as described above.

Data availability

Species resequencing

A. barnebyi (SRRxxxxxx), *A. aurea* (SRR405095), *A. vulgaris* (SRR404349), *A. sibirica* (SRR405090), *A. formosa* (SRR408554), *A. japonica* (SRR413499), *A. oxysepala* (SRR413921), *A. longissima* (SRRXXXXXX), *A. chrysantha* (SRR408559), *A. pubescens* (SRRXXXXxx (GMI - D14R)) are available in the Short Read Archive (https://www.ncbi.nlm.nih.gov/sra).

Whole genome *Aquilegia coerulea* 'Goldsmith'

Sanger sequences used for genome assembly are available in the NCBI Trace Archive (https://www.ncbi.nlm.ni

Aquilegia coerulea 'Goldsmith' ESTs

Available in the NCBI Short Read Archive (SRR505574-SRR505578)

Aquilegia formosa 412 ESTs

Available in the NCBI dbEST (https://www.ncbi.nlm.nih.gov/dbEST/)

Aquilegia coerulea 'Goldsmith' X *Aquilegia chrysantha* mapping population

Available in the NCBI Short Read Archive: SRRXXXXX - SRRXXXXXXX

Aquilegia formosa x *Aquilegia pubescens* mapping population

Available in the NCBI Short Read Archive : SRRXXXXX - SRRXXXXXX (JGI) and SRRXXXXX - SRRXXXXXX (GMI)

RNAseq

Available in the NCBI Short Read Archive: SRRXXXXX - SRRXXXXXX (UCSB)

Other files

vcfs of variants called in the *Aquilegia* species samples (both with and without *S. adoxoides*) are available for download at www.xxxxx.gmi.oeaw.ac.at.

URLs

The *A. coerulea* 'Goldsmith' v3.1 genome release is available at: https://phytozome.jgi.doe.gov/

Acknowledgements

The authors would like to thank Daniel Rokhsar for guidance in initiating the study and Todd Perkins of Goldsmith Seeds (now part of Syngenta) for providing *A. coerulea* 'Goldsmith' seeds. Next generation sequencing of some components of the *Aquilegia formosa* x *Aquilegia pubescens* mapping population was performed at the Vienna Biocenter Core Facilities Next Generation Sequencing (VBCF NGS) unit in Vienna, Austria (http://www.vbcf.ac.at). This work used the Vincent J. Coates Genomics Sequencing Laboratory at UC Berkeley, supported by NIH S10 Instrumentation Grants S10RR029668 and S10RR027303. The work conducted by the U.S. Department of Energy Joint Genome Institute is supported by the Office of Science of the U.S. Department of Energy under Contract No. DE-AC02-05CH11231. T.M. and M.A.L. were supported by the Czech Science Foundation (grant no. P501/12/G090) and the CEITEC 2020 (grant no. LQ1601) project. M.K. was supported by National Program of Sustainability I (grant no. LO1204). G.A was supported by the Austrian Science Funds (FWF DK W1225-B20). E.S.B. was supported by the National Institutes of Health under the Ruth L. Kirschstein National Research Service Award (F32GM103154).

Author contributions statement

M.N. and S.A.H. conceived the study; J.S., J.J., J.G., U.H., and K.B sequenced and assembled the reference; S.S. and. R.H. annotated the reference; G.A. performed coalescent-based modelling; E.B. performed F2 mapping; N.D. contributed RNAseq data and analysis; T.M and M.A.L. performed cytology; M.K. labeled the oligo paint library; J.Y., S.M, and V.N. constructed and sequenced libraries; D.F. analyzed species resequencing data, performed population genetics, and wrote the manuscript (with input from M.N., G.A., A.B., N.D. S.A.H., T.M., and M.A.L.); All authors read and approved the manuscript.

Figures and Tables

List of figure supplementals

- Figure 1-figure supplemental 1. Origin of species samples used for sequencing
- Figure 2-figure supplemental 1. Polymorphism across the genome in all ten species samples
- Figure 2-figure supplemental 2. Species and chromosome trees of *Aquilegia*
- Figure 3-figure supplemental 1. Proportion of significantly-varying subtrees by chromosome
- Figure 3-figure supplemental 2. *P*-values of proportion tests by chromosome for significantly-different trees
- Figure 3-figure supplemental 3. Subtree prevalence across chromosomes for the nine significantly-different subtrees
- Figure 4-figure supplemental 1. Sharing pattern percentages by pattern type
- Figure 6-figure supplemental 1. Model output for all three gene flow scenarios
- Figure 6-figure supplemental 2. Tree topology proportions simulated under assymmetric and unidirectional models
- Figure 7-figure supplemental 1. Polymorphism in the *A. formosa x A. pubescens* mapping population
- Figure 7-figure supplemental 2. Distribution of gene expression values by chromosome
- Figure 8-figure supplemental 1. Immunodetection of anti-5mC antibody

List of Supplementary files

- Supplementary File 1. Genomic libraries included in the *A. coerulea* genome assembly and their respective assembled sequence coverage levels in the *A. coerulea* v3.1 release
- Supplementary File 2. Summary statistics of the output of the whole genome shotgun assembly prior to screening, removal of organelles and contaminating scaffolds and chromosome-scale pseudomolecule construction
- Supplementary File 3. Final summary assembly statistics for chromosome-scale assembly
- Supplementary File 4. Placement of the individual BAC clones and their contribution to the overall error rate
- Supplementary File 5. RNAseq data sets used for gene annotation
- Supplementary File 6. Ratio of polymorphism or divergence on each chromosome versus genome-wide for each species
- Supplementary File 7. Robustness of nucleotide diversity patterns to copy number variant detection methods
- Supplementary File 8. Repeat family prevalence and permutation results in the *A. coerulea* v3.1 genome release
- Supplementary File 9. *K*-mer based estimates of genome size and repetitive sequence proportion
- Supplementary File 10. Mean and median coverage by species
- Supplementary File 11. Proportion of sites removed by each filter - initial filtration without *Semiaquilegia*

- Supplementary File 12. Proportion of sites removed by each filter - final filtration with *Semi-aquilegia*
- Supplementary File 13. Number of derived variants by species
- Supplementary File 14. Transition matrix for the Five-State Markov process
- Supplementary File 15. Transition matrix for the Eight-State Markov process

List of source data files

- Figure5-source data 1 (D statistics)
- Figure7-source data 1 (Physical and genetic distance for *A.formosa x A. pubescens* markers)
- Others??

References

Picard Tools - By Broad Institute; 2018. http://broadinstitute.github.io/picard/.

Aköz G, Nordborg M. Genome duplication and reorganization in Aquilegia. bioRxiv. 2018; BIORXIV/2018/407973.

Avise JC, Robinson TJ. Hemiplasy: A new term in the lexicon of phylogenetics. Systematic Biology. 2008; 57(3):503–507.

Bastida JM, Alcántara JM, Rey PJ, Vargas P, Herrera CM. Extended phylogeny of *Aquilegia*: The biogeographical and ecological patterns of two simultaneous but contrasting radiations. Plant Systematics and Evolution. 2010; 284(3):171–185.

Baym M, Kryazhimskiy S, Lieberman T, Chung H, Desai MM, Kishony R. Inexpensive Multiplexed Library Preparation for Megabase-Sized Genomes. PLoS One. 2015; 10:e0128036.

Bennett MD, Leitch IJ. Nuclear DNA amounts in angiosperms: targets, trends and tomorrow. Annals of Botany. 2011; 107(3):467. doi: 10.1093/AOB/MCQ258.

Bennett MD, Smith JB, Heslop-Harrison JS. Nuclear DNA Amounts in Angiosperms. Proceedings of the Royal Society B: Biological Sciences. 1982; 216(1203):179–199. doi: 10.1098/rspb.1982.0069.

Broman KW, Wu H, Sen Ś, Churchill GA. R/qtl: QTL mapping in experimental crosses. Bioinformatics. 2003 may; 19(7):889–890.

Cazaux B, Catalan J, Veyrunes F, Douzery EJ, Britton-Davidian J. Are ribosomal DNA clusters rearrangement hotspots? A case study in the genus *Mus* (Rodentia, Muridae). BMC Evolutionary Biology. 2011; 11(1):124.

Cingolani P, Platts A, Coon M, Nguyen T, Wang L, Land SJ, Lu X, Ruden DM. A program for annotating and predicting the effects of single nucleotide polymorphisms, SnpEff: SNPs in the genome of Drosophila melanogaster strain w1118; iso-2; iso-3. Fly. 2012; 6(2):80–92.

Cooper EA, Whittall JB, Hodges SA, Nordborg M. Genetic variation at nuclear loci fails to distinguish two morphologically distinct species of *Aquilegia*. PLoS ONE. 2010; 5(1).

Corbett-Detig RB, Hartl DL, Sackton TB. Natural Selection Constrains Neutral Diversity across A Wide Range of Species. PLOS Biology. 2015 apr; 13(4):e1002112. http://dx.plos.org/10.1371/journal.pbio.1002112, doi: 10.1371/journal.pbio.1002112.

Cossard G, Sannier J, Sauquet H, Damerval C, de Craene LR, Jabbour F, Nadot S. Subfamilial and tribal relationships of Ranunculaceae: evidence from eight molecular markers. Plant Systematics and Evolution. 2016; 302(4):419–431.

Coyne JA, Orr AH, Orr HA. Speciation. Sunderland, Massachusetts: Sinauer; 2004.

Cui L, Wall PK, Leebens-Mack JH, Lindsay BG, Soltis DE, Doyle JJ, Soltis PS, Carlson JE, Arumuganathan K, Barakat A, Albert VA, Ma H, DePamphilis CW. Widespread genome duplications throughout the history of flowering plants. Genome Research. 2006; 16(6):738–749.

DePristo M, Banks E, Poplin R, Garimella K, Maguire J, Al E. A framework for variation discovery and genotyping using next-generation DNA sequencing data. Nature Genetics. 2011; (43):491–498.

Durand EY, Patterson N, Reich D, Slatkin M. Testing for ancient admixture between closely related populations. Molecular biology and evolution. 2011 aug; 28(8):2239–52. http://www.ncbi.nlm.nih.gov/pubmed/21325092http://www.pubmedcentral.nih.gov/articlerender.fcgi?artid=PMC3144383, doi: 10.1093/molbev/msr048.

Fior S, Li M, Oxelman B, Viola R, Hodges SA, Ometto L, Varotto C. Spatiotemporal reconstruction of the *Aquilegia* rapid radiation through next-generation sequencing of rapidly evolving cpDNA regions. New Phytologist. 2013; 198(2):579–592.

Grant V. Isolation and hybridization between Aquilegia formosa and A. pubescens. Aliso. 1952; 2:341–360.

Green DM. Muller's Ratchet and the evolution of supernumerary chromosomes. Genome. 1990 dec; 33(6):818–824. doi: 10.1139/g90-123.

Green RE, Krause J, Briggs AW, Maricic T, Stenzel U, Kircher M, Patterson N, Li H, Zhai W, Fritz MHY, Hansen NF, Durand EY, Malaspinas AS, Jensen JD, Marques-Bonet T, Alkan C, Prufer K, Meyer M, Burbano HA, Good JM, et al. A Draft Sequence of the Neandertal Genome. Science. 2010; 328(5979):710–722.

Haas BJ, Delcher AL, Wortman JR, Salzberg SL. DAGchainer: a tool for mining segmental genome duplications and synteny. Bioinformatics. 2004; 20(18):3643–3646.

Haas BJ, Delcher AL, Mount S M SM, Wortman JR, Smith RK, Hannick LI, Maiti R, Ronning CM, Rusch DB, Town CD, Salzberg SL, White O. Improving the Arabidopsis genome annotation using maximal transcript alignment assemblies. Nucleic Acids Research. 2003; 31(19):5654–5666.

Han Y, Zhang T, Thammapichai P, Weng Y, Jiang J. Chromosome-specific painting in Cucumis species using bulked oligonucleotides. Genetics. 2015; 200(3):771–779.

Herlihy CR, Eckert CG. Genetic cost of reproductive assurance in a self-fertilizing plant. Nature. 2002 mar; 416(6878):320–323.

Hizume M, Shiraishi H, Matsusaki Y, Shibata F. Localization of 45S and 5S rDNA on chromosomes of *Nigella damascena*, Ranunculaceae. CYTOLOGIA. 2013; 78(4):379–381.

Hodges SA, Arnold ML. Columbines - a geographically widespread species flock. Proceedings of the National Academy of Sciences of the United States of America. 1994; 91(11):5129–5132.

Hodges SA, Arnold ML. Floral and ecological isolation between *Aquilegia formosa* and *Aquilegia pubescens*. Proceedings of the National Academy of Sciences of the United States of America. 1994; 91(March):2493–2496.

Hodges SA, Derieg NJ. Adaptive radiations: from field to genomic studies. Proceedings of the National Academy of Sciences of the United States of America. 2009; 106 Suppl:9947–9954.

Hodges SA, Fulton M, Yang JY, Whittall JB. Verne Grant and evolutionary studies of *Aquilegia*. New Phytologist. 2004; 161(1):113–120.

Hodges SA, Whittall JB, Fulton M, Yang JY. Genetics of floral traits influencing reproductive isolation between *Aquilegia formosa* and *Aquilegia pubescens*. The American naturalist. 2002; 159 Suppl(May):S51–S60.

Huang J, Ma L, Yang F, Fei SZ, Li L. 45S rDNA regions are chromosome fragile sites expressed as gaps in vitro on metaphase chromosomes of root-tip meristematic cells in Lolium spp. PLoS ONE. 2008; 3(5).

Hudson RR, Slatkin M, Maddison WP. Estimation of levels of gene flow from DNA sequence data. Genetics. 1992; 132(2):583–9.

Jaffe DB, Butler J, Gnerre S, Mauceli E, Lindblad-Toh K, Mesirov JP, Zody MC, Lander ES. Whole-genome sequence assembly for mammalian genomes: Arachne 2. Genome Research. 2003; 13(1):91–96.

Jones RN. B chromosomes in plants. New Phytologist. 1995; 131(4):411–434. doi: 10.1111/j.1469-8137.1995.tb03079.x.

Karasov TL, Horton MW, Bergelson J. Genomic variability as a driver of plant-pathogen coevolution? Current Opinion in Plant Biology. 2014; 18(1):24–30.

Kent WJ. BLAT - The BLAST-like alignment tool. Genome Research. 2002; 12(4):656–664.

Kimura M. The Neutral Theory of Molecular Evolution. Cambridge: Cambridge University Press; 1983.

Kocsis E, Trus BL, Steer CJ, Bisher ME, Steven AC. Image Averaging of Flexible Fibrous Macromolecules: The Clathrin Triskelion Has an Elastic Proximal Segment. Journal of Structural Biology. 1991; 107:6–14.

Korneliussen TS, Albrechtsen A, Nielsen R. ANGSD: Analysis of Next Generation Sequencing Data. BMC Bioinformatics. 2014; 15(1):356.

Kramer E, Hodges S. *Aquilegia* as a model system for the evolution and ecology of petals. Philosophical transactions of the Royal Society of London Series B, Biological sciences. 2010; 365(1539):477–490.

Kramer EM. *Aquilegia*: a new model for plant development, ecology, and evolution. Annual review of plant biology. 2009; 60:261–277.

Lamichhaney S, Berglund J, Almén MS, Maqbool K, Grabherr M, Martinez-Barrio A, Promerová M, Rubin CJ, Wang C, Zamani N, Grant BR, Grant PR, Webster MT, Andersson L. Evolution of Darwin's finches and their beaks revealed by genome sequencing. Nature. 2015; 518(7539):371–375.

Langlet O. Beiträge zur Zytologie der Ranunculazeen. Svenk Botanisk Tidskrift. 1927; 21(1):1–17.

Langlet O. Über Chromosomenverhaltnisse und Systematik der Ranununculaceae. Svenk Botanisk Tidskrift. 1932; 26(11):1–2.

Leffler EM, Bullaughey K, Matute DR, Meyer WK, Ségurel L, Venkat A, Andolfatto P, Przeworski M. Revisiting an old riddle: what determines genetic diversity levels within species? PLoS Biology. 2012; 10(9).

Li H. Aligning sequence reads, clone sequences and assembly contigs with BWA-MEM. arXiv:13033997v1 [q-bioGN]. 2013; .

Li H, Durbin R. Fast and accurate short read alignment with Burrows-Wheeler transform. Bioinformatics. 2009; 25(14):1754–1760.

Li H, Handsaker B, Wysoker A, Fennell T, Ruan J, Homer N, Marth G, Abecasis G, Durbin R. The Sequence Alignment/Map format and SAMtools. Bioinformatics. 2009; 25(16):2078–2079.

Li LF, Wang HY, Pang D, Liu Y, Liu B, Xiao HX. Phenotypic and genetic evidence for ecological speciation of *Aquilegia japonica* and *A. oxysepala*. New Phytologist. 2014; 204(4):1028–1040.

Liao L, Xu L, Zhang D, Fang L, Deng H, Shi J, Li T. Multiple hybridization origin of *Ranunculus cantoniensis* (4x): Evidence from trnL-F and ITS sequences and fluorescent in situ hybridization (FISH). Plant Systematics and Evolution. 2008; 276(1-2):31–37.

Linnert G. Cytologische Untersuchungen an Arten und Artenbastarden von *Aquilegia* - I. Struktur und Polymorphismus der Nukleolen-chromosomen, Quadrivalente und B-chromosomen. Chromosoma. 1961; 12:449–459.

Loh YHE, Bezault E, Muenzel FM, Roberts RB, Swofford R, Barluenga M, Kidd CE, Howe AE, Di Palma F, Lindblad-Toh K, Hey J, Seehausen O, Salzburger W, Kocher TD, Streelman JT. Origins of shared genetic variation in African cichlids. Molecular biology and evolution. 2013 apr; 30(4):906–17.

Lyons E, Freeling M. How to usefully compare homologous plant genes and chromosomes as DNA sequences. The Plant Journal. 2008; 53(4):661–673.

Malinsky M, Svardal H, Tyers AM, Miska EA, Genner MJ, Turner GF, Durbin R. Whole Genome Sequences Of Malawi Cichlids Reveal Multiple Radiations Interconnected By Gene Flow. bioRxiv. 2017 dec; p. 143859.

Mallet J, Besansky N, Hahn MW. How reticulated are species? BioEssays. 2016; 38(2):140–149.

Mandáková T, Lysak MA, Mandáková T, Lysak MA. Painting of Arabidopsis Chromosomes with Chromosome-Specific BAC Clones. In: *Current Protocols in Plant Biology* Hoboken, NJ, USA: John Wiley & Sons, Inc.; 2016.p. 359–371. doi: 10.1002/cppb.20022.

Marçais G, Kingsford C. A fast, lock-free approach for efficient parallel counting of occurrences of k-mers. Bioinformatics. 2011 mar; 27(6):764–770. https://academic.oup.com/bioinformatics/article-lookup/doi/10.1093/bioinformatics/btr011, doi: 10.1093/bioinformatics/btr011.

McCarthy DJ, Chen Y, Smyth GK. Differential expression analysis of multifactor RNA-Seq experiments with respect to biological variation. Nucleic Acids Research. 2012 may; 40(10):4288–4297.

McKenna A, Hanna M, Banks E, Sivachenko A, Cibulskis K, Kernytsky A, Garimella K, Altshuler D, Gabriel S, Daly M, DePristo MA. The genome analysis toolkit: A MapReduce framework for analyzing next-generation DNA sequencing data. Genome Research. 2010; 20(9):1297–1303.

McVean GA, Altshuler (Co-Chair) DM, Durbin (Co-Chair) RM, Abecasis GR, Bentley DR, Chakravarti A, Clark AG, Donnelly P, Eichler EE, Flicek P, Gabriel SB, Gibbs RA, Green ED, Hurles ME, Knoppers BM, Korbel JO, Lander ES, Lee C, Lehrach H, Mardis ER, et al. An integrated map of genetic variation from 1,092 human genomes. Nature. 2012 oct; 491(7422):56–65.

Melters DP, Bradnam KR, Young HA, Telis N, May MR, Ruby J, Sebra R, Peluso P, Eid J, Rank D, Garcia J, DeRisi JL, Smith T, Tobias C, Ross-Ibarra J, Korf I, Chan SW. Comparative analysis of tandem repeats from hundreds of species reveals unique insights into centromere evolution. Genome Biology. 2013 jan; 14(1):R10.

Miller CA, Hampton O, Coarfa C, Milosavljevic A. ReadDepth: A parallel R package for detecting copy number alterations from short sequencing reads. PLoS ONE. 2011 jan; 6(1):e16327.

Ming R, Bendahmane A, Renner SS. Sex chromosomes in land plants. Annual Review of Plant Biology. 2011; 62(1):485–514.

Mlinarec J, Papeš DA, Besendorfer V. Ribosomal, telomeric and heterochromatin sequences localization in the karyotype of *Anemone hortensis*. Botanical Journal of the Linnean Society. 2006; 150(2):177–186.

Montalvo AM. Inbreeding Depression and Maternal Effects in *Aquilegia caerulea*, a Partially Selfing Plant. Ecology. 1994 dec; 75(8):2395.

Munz PA. *Aquilegia*: The Cultivated and Wild Columbines. Gentes herbarum. 1946; 7:1–150.

Murgha YE, Rouillard JM, Gulari E. Methods for the preparation of large quantities of complex single-stranded oligonucleotide libraries. PLoS ONE. 2014 apr; 9(4):e94752.

Nam K, Munch K, Hobolth A, Dutheil JY, Veeramah KR, Woerner AE, Hammer MF, Mailund T, Schierup MH, Schierup MH. Extreme selective sweeps independently targeted the X chromosomes of the great apes. Proceedings of the National Academy of Sciences. 2015 may; 112(20):6413–6418.

Nordborg M, Innan H. The genealogy of sequences containing multiple sites subject to strong selection in a subdivided population. Genetics. 2003 mar; 163(3):1201–13.

Novikova PY, Hohmann N, Nizhynska V, Tsuchimatsu T, Ali J, Muir G, Guggisberg A, Paape T, Schmid K, Fedorenko OM, Holm S, Säll T, Schlötterer C, Marhold K, Widmer A, Sese J, Shimizu KK, Weigel D, Krämer U, Koch MA, et al. Sequencing of the genus *Arabidopsis* identifies a complex history of nonbifurcating speciation and abundant trans-specific polymorphism. Nature Genetics. 2016; 48(9):1077–1082.

Paradis E, Claude J, Strimmer K. APE: analyses of phylogenetics and evolution in R language. Bioinformatics. 2004; 20:289–290.

Pease JB, Haak DC, Hahn MW, Moyle LC. Phylogenomics reveals three sources of adaptive variation during a rapid radiation. PLoS Biology. 2016; 14(2).

R Core Team. R: A Language and Environment for Statistical Computing. R Foundation for Statistical Computing, Vienna, Austria; 2014, http://www.R-project.org/.

Rabanal FA, Nizhynska V, Mandáková T, Novikova PY, Lysak MA, Mott R, Nordborg M. Unstable Inheritance of 45S rRNA Genes in Arabidopsis thaliana. G3 (Bethesda, Md). 2017 apr; 7(4):1201–1209.

Ro KE, Keener CS, McPheron Ba. Molecular phylogenetic study of the Ranunculaceae: utility of the nuclear 26S ribosomal DNA in inferring intrafamilial relationships. Molecular phylogenetics and evolution. 1997; 8(2):117–127.

Ro KE, Mcpheron BA. Molecular phylogeny of the *Aquilegia* group (Ranunculaceae) based on internal transcribed spacers and 5.8S nuclear ribosomal DNA. Biochemical Systematics and Ecology. 1997; 25(5):445–461.

Roa F, Guerra M. Distribution of 45S rDNA sites in chromosomes of plants: Structural and evolutionary implications. BMC Evolutionary Biology. 2012; 12(1):225.

Robinson MD, McCarthy DJ, Smyth GK. edgeR: a Bioconductor package for differential expression analysis of digital gene expression data. Bioinformatics. 2010 jan; (1):139–140.

Salamov AA, Solovyev VV. Ab initio gene finding in Drosophila genomic DNA. Genome Research. 2000; 10(4):516–522.

Schliep KP. phangorn: phylogenetic analysis in R. Bioinformatics. 2011; 27(4):592–593.

Schluter D, Conte GL. Genetics and ecological speciation. Proceedings of the National Academy of Sciences. 2009; 106(Supplement_1):9955–9962.

Schluter D. The Ecology of Adaptive Radiation. New York: Oxford University Press; 2000.

Schumer M, Xu C, Powell D, Durvasula A, Skov L, Holland C, Sankararaman S, Andolfatto P, Rosenthal G, Przeworski M. Natural selection interacts with the local recombination rate to shape the evolution of hybrid genomes; 2017.

Seehausen O, Butlin RK, Keller I, Wagner CE, Boughman JW, Hohenlohe PA, Peichel CL, Saetre GP, Bank C, Brännström Å, Brelsford A, Clarkson CS, Eroukhmanoff F, Feder JL, Fischer MC, Foote AD, Franchini P, Jiggins CD, Jones FC, Lindholm AK, et al. Genomics and the origin of species. Nature Reviews Genetics. 2014; 15(3):176–192.

Shu S, Goodstein D, Rokhsar D, PERTRAN: Genome-guided RNA-seq Read Assembler. - Report Number: LBNL-7081E; 2013.

Smit A, Hubley R, RepeatModeler Open-1.0; 2008-2015. www.repeatmasker.org.

Smit A, Hubley R, Green P, RepeatMasker Open-4.0. 2013-2015; 2013-2015. http://www.repeatmasker.org.

Soza VL, Brunet J, Liston A, Salles Smith P, Di Stilio VS. Phylogenetic insights into the correlates of dioecy in meadow-rues (*Thalictrum*, Ranunculaceae). Molecular Phylogenetics and Evolution. 2012; 63(1):180–192.

Spedicato GA. Discrete Time Markov Chains with R. The R Journal. 2017 07; https://journal.r-project.org/archive/2017/RJ-2017-036/index.html, r package version 0.6.9.7.

Stamatakis A. RAxML version 8: a tool for phylogenetic analysis and post-analysis of large phylogenies. Bioinformatics. 2014 may; 30(9):1312–1313.

Sun H, Ding J, Piednoël M, Schneeberger K, Birol I. findGSE: estimating genome size variation within human and Arabidopsis using k-mer frequencies. Bioinformatics. 2018 feb; 34(4):550–557. https://academic.oup.com/bioinformatics/article/34/4/550/4386918, doi: 10.1093/bioinformatics/btx637.

Svardal H, Jasinska AJ, Apetrei C, Coppola G, Huang Y, Schmitt CA, Jacquelin B, Ramensky V, Müller-Trutwin M, Antonio M, Weinstock G, Grobler JP, Dewar K, Wilson RK, Turner TR, Warren WC, Freimer NB, Nordborg M. Ancient hybridization and strong adaptation to viruses across African vervet monkey populations. Nature Genetics. 2017 oct; 49(12):1705–1713.

Takahata N. Gene genealogy in three related populations: Consistency probability between gene and population trees. Genetics. 1989 aug; 122(4):957–66.

Taylor RJ. Interspecific hybridization and its evolutionary significance in the genus *Aquilegia*. Brittonia. 1967; 19(4):374.

Tiley GP, Ané C, Burleigh JG. Evaluating and characterizing ancient whole-genome duplications in plants with gene count data. Genome biology and evolution. 2016; 8(4):1023–1037.

Toups MA, Hahn MW. Retrogenes reveal the direction of sex-chromosome evolution in mosquitoes. Genetics. 2010 oct; 186(2):763–766.

Valente GT, Nakajima RT, Fantinatti BEA, Marques DF, Almeida RO, Simões RP, Martins C. B chromosomes: from cytogenetics to systems biology. Chromosoma. 2017; 126(1):73–81. doi: 10.1007/s00412-016-0613-6.

Vanneste K, Baele G, Maere S, Van De Peer Y. Analysis of 41 plant genomes supports a wave of successful genome duplications in association with the Cretaceous-Paleogene boundary. Genome Research. 2014; 24(8):1334–1347.

Vicoso B, Bachtrog D. Reversal of an ancient sex chromosome to an autosome in Drosophila. Nature. 2013; 499(7458):332–335.

Wang W, Lu AM, Ren Y, Endress ME, Chen ZD. Phylogeny and classification of Ranunculales: Evidence from four molecular loci and morphological data. Perspectives in Plant Ecology, Evolution and Systematics. 2009; 11(2):81–110.

Weiss-Schneeweiss H, Schneeweiss GM, Stuessy TF, Mabuchi T, Park JM, Jang CG, Sun BY. Chromosomal stasis in diploids contrasts with genome restructuring in auto- and allopolyploid taxa of *Hepatica* (Ranunculaceae). New Phytologist. 2007; 174(3):669–682.

Westergaard M. The Mechanism of Sex Determination in Dioecious Flowering Plants. Advances in Genetics. 1958; 9(C):217–281.

Whittall JB, Hodges SA. Pollinator shifts drive increasingly long nectar spurs in columbine flowers. Nature. 2007; 447(7145):706–709.

Yang JY, Hodges Sa. Early Inbreeding depression selects for high outcrossing rates in *Aquilegia formosa* and *Aquilegia pubescens*. International Journal Of Plant Sciences. 2010; 171(8):860–871.

Yeh RF, Lim LP, Burge CB. Computational inference of homologous gene structures in the human genome. Genome research. 2001 may; 11(5):803–16.

Figure 1-figure supplemental 1. Origin of species samples used for sequencing.

Species	Native range	Collection locality	Tissue source
Aquilegia aurea	Europe	Bulgaria	wild
A. barnebyi	North America	Colorado, USA	grown from wild seed
A. chrysantha	North America	Arizona, USA	wild
A. formosa	North America	California, USA	wild
A. japonica	Asia	Jilin, China	wild
A. longissima	North America	Texas, USA	unknown
A. oxysepala var. oxysepala	Asia	Heilongjiang, China	wild
A. pubescens	North America	California, USA	wild
A. sibirica	Asia	Khazakhstan	grown from wild seed
A. vulgaris	Europe	Switzerland	wild
Semiaquilegia adoxoides	Asia	China	grown from wild seed

Figure 2-figure supplemental 1. Polymorphism across the genome in all ten species samples. Polymorphism in 1Mb windows across the genome for all ten species samples. Some samples show long stretches of homozygosity indicative of recent inbreeding; this inbreeding could explain the lack of increased polymorphism on chromosome four in *A. aurea*. Similarly, an extended stretch of homozygosity was seen on chromosome four in an additional sample of *A. pubescens* that was used in the construction of our F2 mapping population (**Figure 7-figure supplemental 2**, sample pub.1).

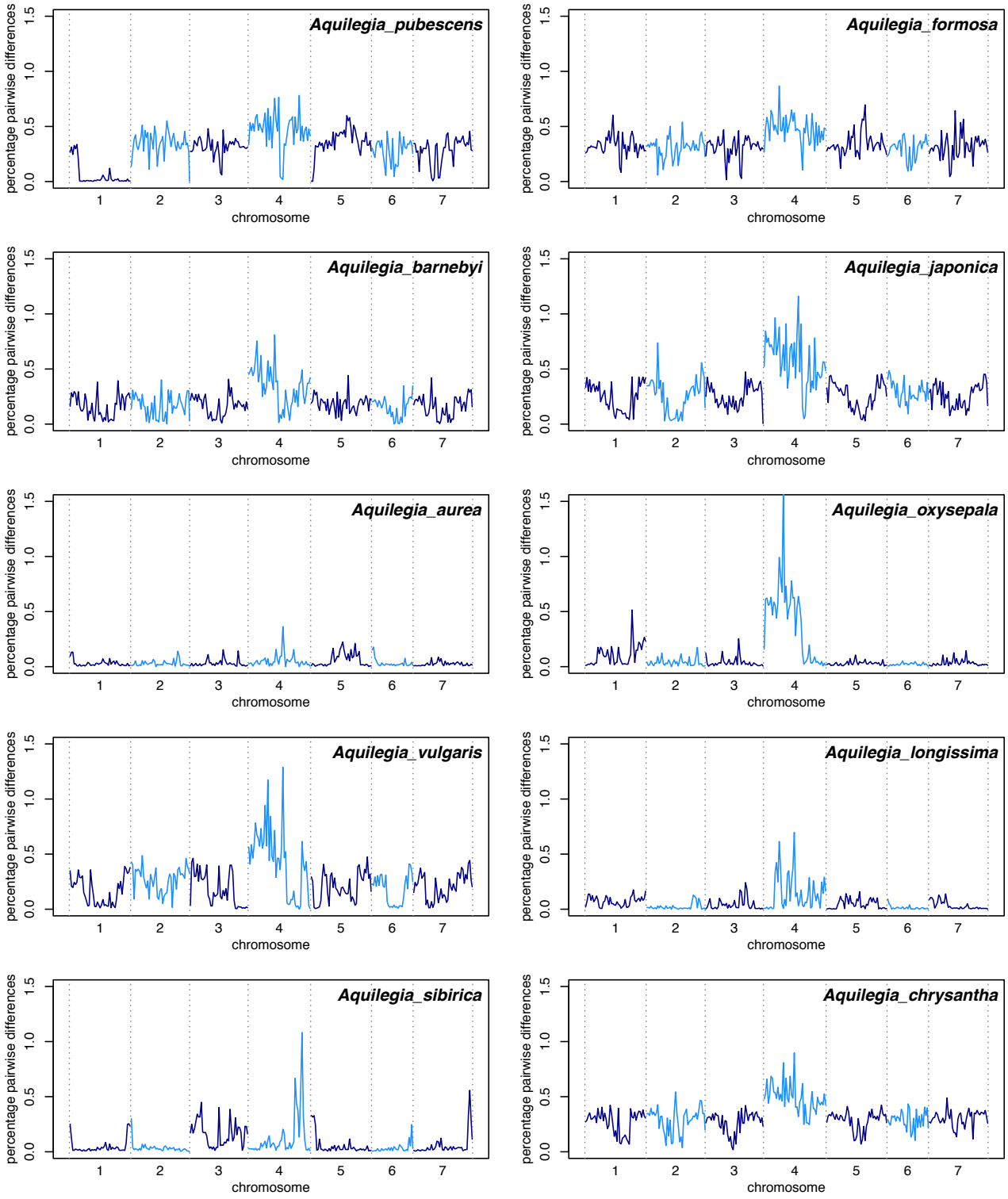

Figure 2-figure supplemental 2. Species and chromsome trees of *Aquilegia***.** (a) RAxML tree from concatenated genomic data (b) Neighbor joining tree from concatenated chromosome four data (c) RAxML tree from concatenated chromosome four data. Bootstrap support values are presented for all trees

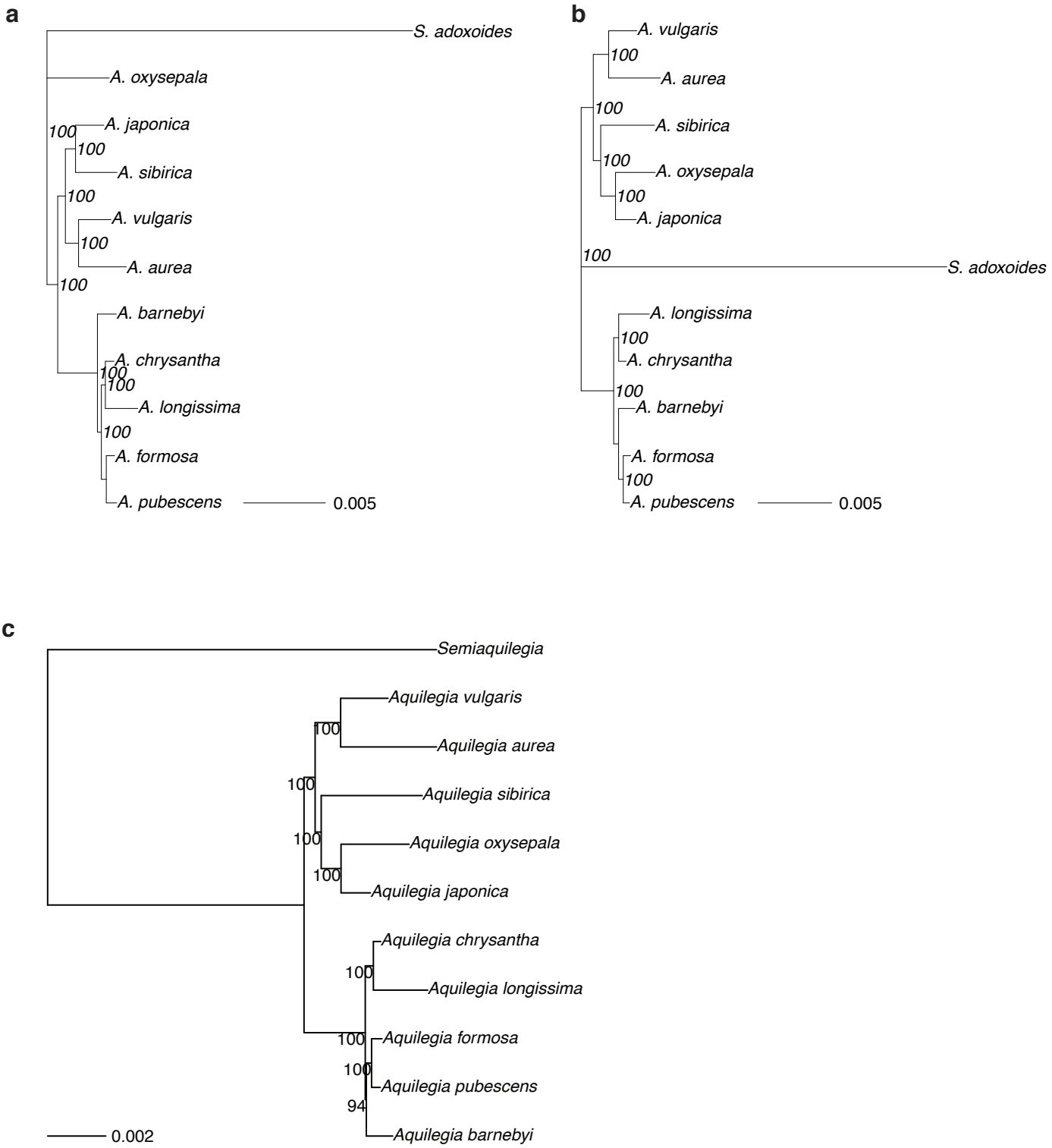

Figure 3-figure supplemental 1. Proportion of significantly-varying subtrees by chromosome - corrected for 217 tests

	Proportion of window trees with subtree								
	Chromosome								
Subtree	1	2	3	4	5	6	7	Genome	Corrected p-val
japon/sib	0.49	0.51	0.47	0.14	0.48	0.53	0.43	0.45	3.7E-19
aur/japon/sib/vul	0.36	0.35	0.31	0.07	0.35	0.38	0.31	0.31	2.4E-12
japon/oxy	0.23	0.24	0.29	0.47	0.25	0.19	0.22	0.26	3.6E-10
oxy basal	0.37	0.29	0.27	0.10	0.32	0.36	0.31	0.30	7.0E-09
N. Americans	0.02	0.05	0.02	0.11	0.03	0.02	0.05	0.04	3.0E-06
aur/japon/oxy	0.01	0.01	0.01	0.05	0.00	0.00	0.00	0.01	2.6E-04
bar/chr/for/lon/pub	0.97	0.97	0.97	0.90	0.98	0.96	0.97	0.96	6.2E-03
bar/pub	0.26	0.12	0.17	0.13	0.13	0.17	0.17	0.17	6.6E-03
japon/oxy/sib	0.09	0.17	0.14	0.24	0.12	0.14	0.14	0.14	2.9E-02
japon/sib/vul	0.10	0.06	0.05	0.02	0.08	0.11	0.10	0.07	3.9E-02

Figure 3-figure supplemental 2. P-values of proportion tests by chromosome for significantly-different trees - corrected for 70 tests

	Corrected p-value						
Subtree	Chr_01	Chr_02	Chr_03	Chr_04	Chr_05	Chr_06	Chr_07
japon/sib	1	1	1	**9.2E-19**	1	0.95	1
aur/japon/sib/vul	1	1	1	**2.3E-13**	1	1	1
japon/oxy	1	1	1	**7.5E-10**	1	1	1
oxy basal	0.3	1	1	**6.7E-09**	1	1	1
oxy/sib	1	1	1	**3.1E-05**	1	1	1
N.America	1	1	1	**3.9E-04**	1	1	1
aur/japon/oxy	1	1	1	**7.5E-04**	1	1	1
japon/oxy/sib	0.7	1	1	**9.9E-03**	1	1	1
japon/sib/vul	1	1	1	8.9E-02	1	1	1
bar/pub	**0.002**	1	1	1	1	1	1

Figure 3-figure supplemental 3. Subtree prevalence across chromosomes for the nine significantly-different subtrees.

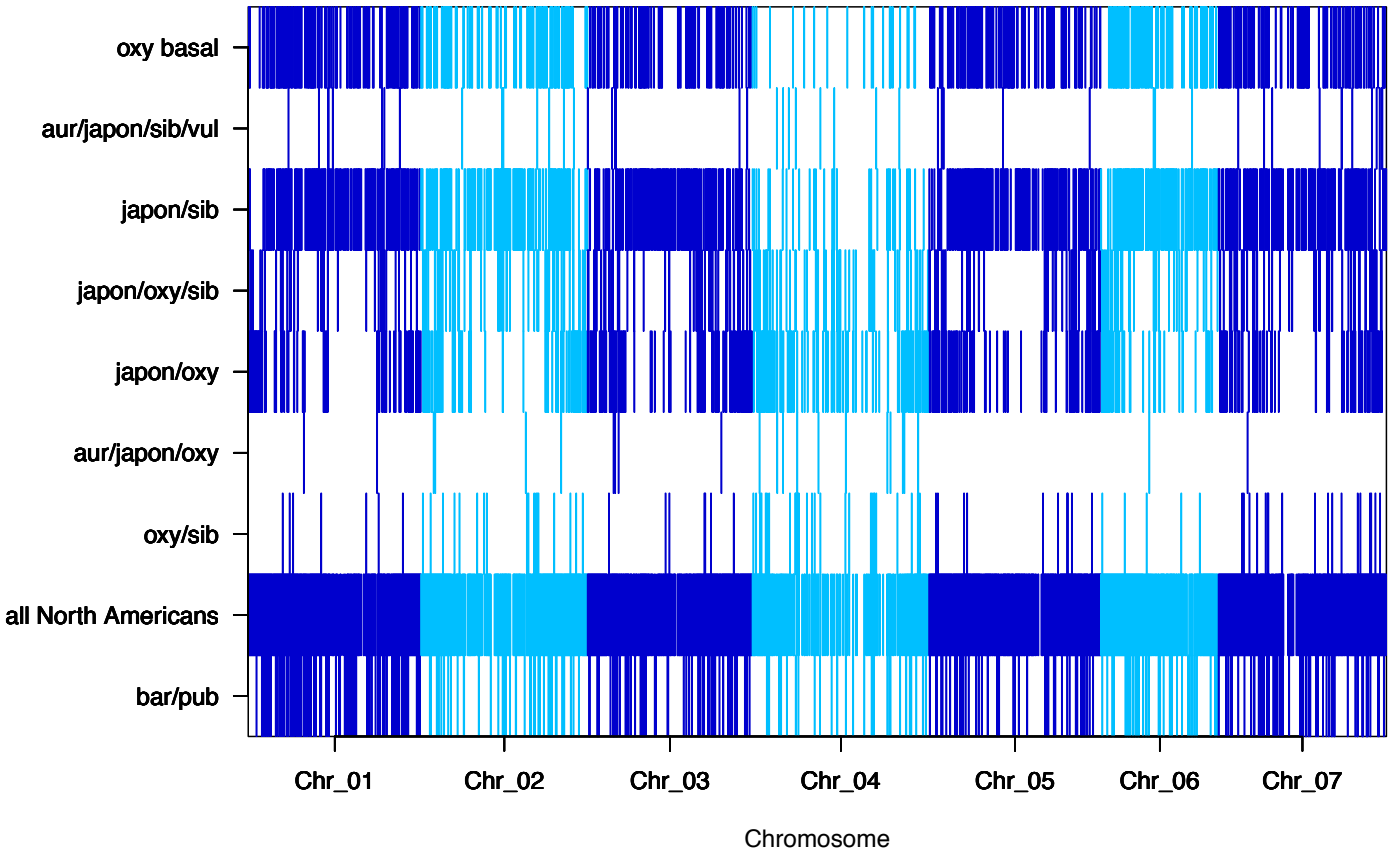

Figure 4-figure supplemental 1. Sharing pattern percentages by pattern type

		Percentage of shared variants							
		Chromosome							
Sharing depth	Sharing pattern	1	2	3	4	5	6	7	genome
shallow	within N.Am	36.4	36.8	37.8	32.9	37.4	36.7	37.2	36.8
	within Asia	10.7	10.6	11.0	12.7	10.6	10.7	10.1	10.8
	within Europe	5.5	5.1	4.4	5.2	4.7	5.2	4.6	4.9
deep	N.Am and Asia	7.4	7.1	7.1	7.6	7.2	6.8	7.0	7.1
	Europe and N.Am	3.3	3.6	3.7	3.7	3.3	3.9	3.3	3.5
	Europe and Asia	14.7	14.2	14.7	13.2	15.1	14.5	15.5	14.7
very deep	among all	22.0	22.6	21.4	24.6	21.7	22.3	22.2	22.2

Figure 6-figure supplemental 1. Model output for all three gene flow scenarios. Simulated tree topology proportions (left) and D-statistics (right) under models of (a) symmetric, (b) asymmetric, and (c) unidirectional gene flow. Left: Tree topologies are simulated under 100 different combinations of m and N (represented as M on the x-axis) and 10 different combinations of t1 (four values of which are shown in the legend). The difference between each of the 1000 simulated and observed tree topology proportions is estimated using euclidean distance where observed and simulated proportions of sib-japon and japon-oxy topologies specify point 1 and point 2, respectively (sib-japon refers to red tree while japon-oxy refers to blue tree in **Fig. 6a**). Quantified as such, a difference of zero (y-axis) points at the best parameter combination that matches observed allele sharing proportions genomewide. Right: Given the "species" tree (**Fig. 6b**), D-statistics (y-axis) are calculated for different combinations of m (x-axis) and N (legend; top left) which cover the parameter space of interest (**Fig. 6c** and **Supplementary Table 7**). Note that simulations are carried out with t1=1 and only five out of twelve N values are shown in the legend. Filled circles on the y-axis denote observed chromosome-specific D statistic estimates and horizontal black lines denote the range of these values

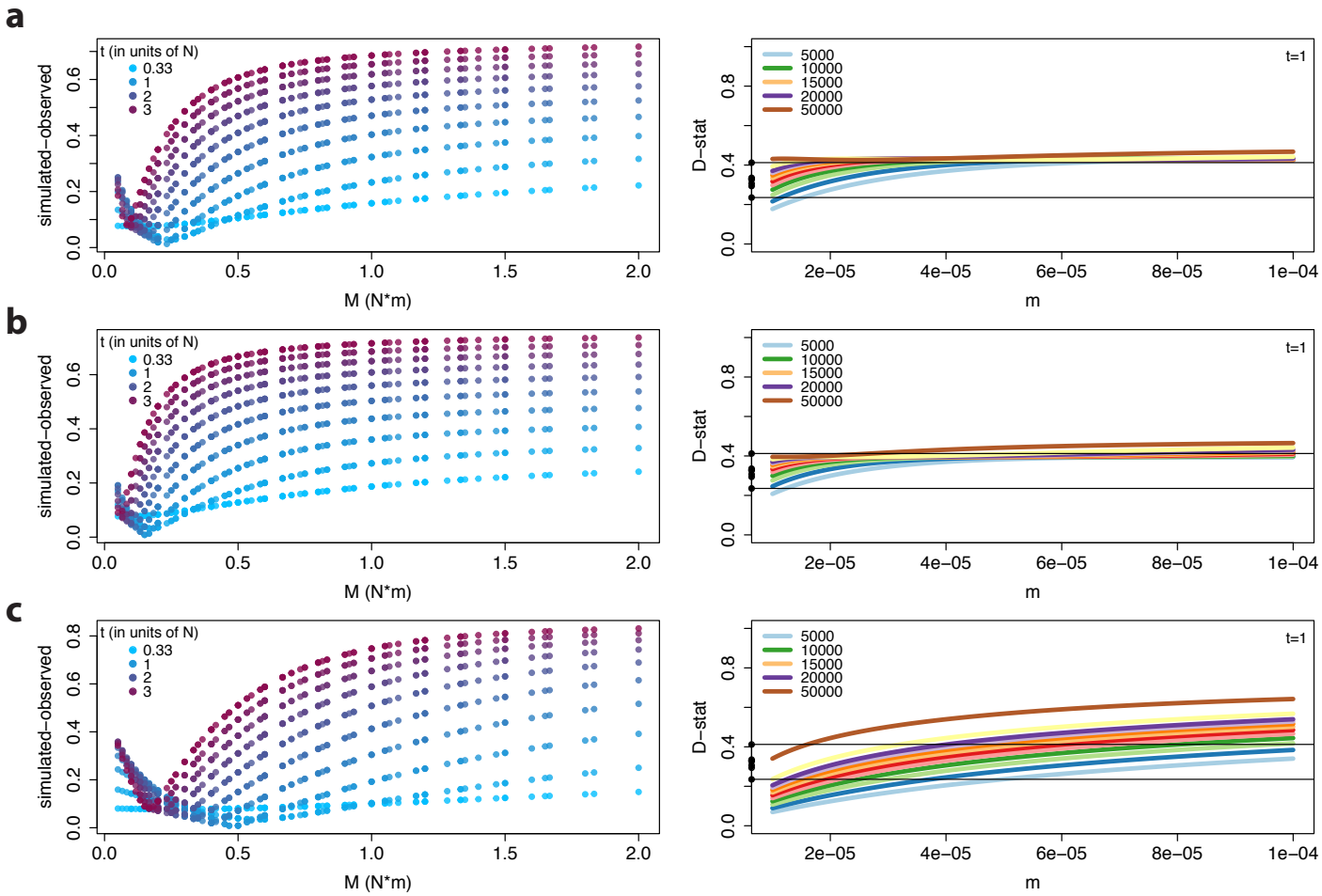

Figure 6-figure supplemental 2. Tree topology proportions simulated under assymmetric and unidirectional models

gene flow	m	N	sib-japon	japon-oxy	sib-oxy	D-stat
asymmetric	$2x10^{-5}$	8333	0.53	0.31	0.15	0.35
	$2x10^{-5}$	16666	0.41	0.40	0.18	0.38
	$4x10^{-5}$	16666	0.30	0.49	0.21	0.40
	$2x10^{-5}$	33332	0.30	0.49	0.21	0.40
unidirectional	$5x10^{-5}$	10000	0.53	0.30	0.15	0.33
	$5x10^{-5}$	20000	0.40	0.43	0.17	0.43
	$7.5x10^{-5}$	20000	0.31	0.51	0.17	0.50
	$5x10^{-5}$	30000	0.31	0.51	0.17	0.50

Figure 7-figure supplemental 1. Polymorphism in the *A. formosa* x *A. pubescens* mapping population. (a) Polymorphism by chromosome for mapping population F0s (form.1, form.2, pub.1, and pub.2) and their corresponding F1s (F1.1 and F1.2). Samples form.2 and pub.2 were included in the main data set as *A. formosa* and *A. pubescens*; they are presented again in this figure for clarity. Although polymorphism was not elevated on chromosome four in pub.1, polymorphism was elevated in an F1 constructed using this individual (F1.1). (c) Polymorphism across the genome in 1MB windows for the samples in (a). A large inbred region observed on chromosome four in F1.1 suggests that inbreeding is the cause of the non-elevated polymorphism in this sample.

a

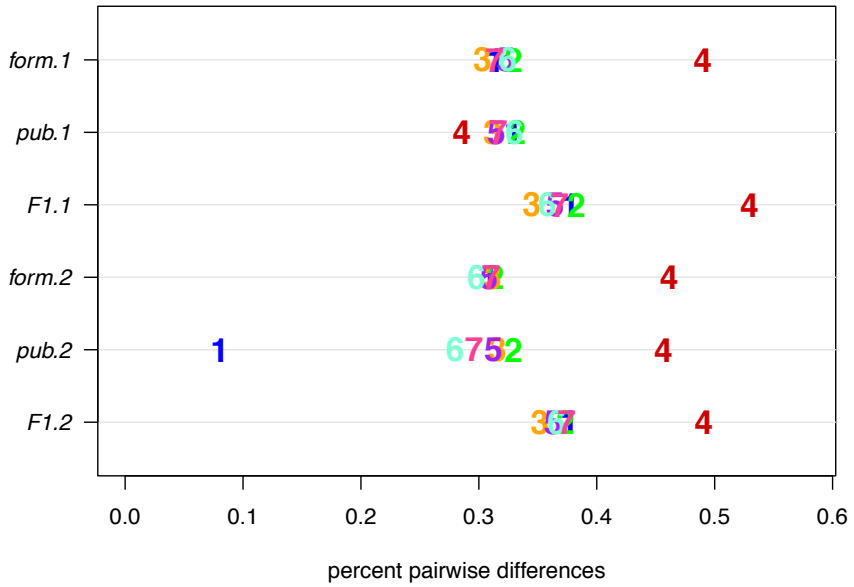

b

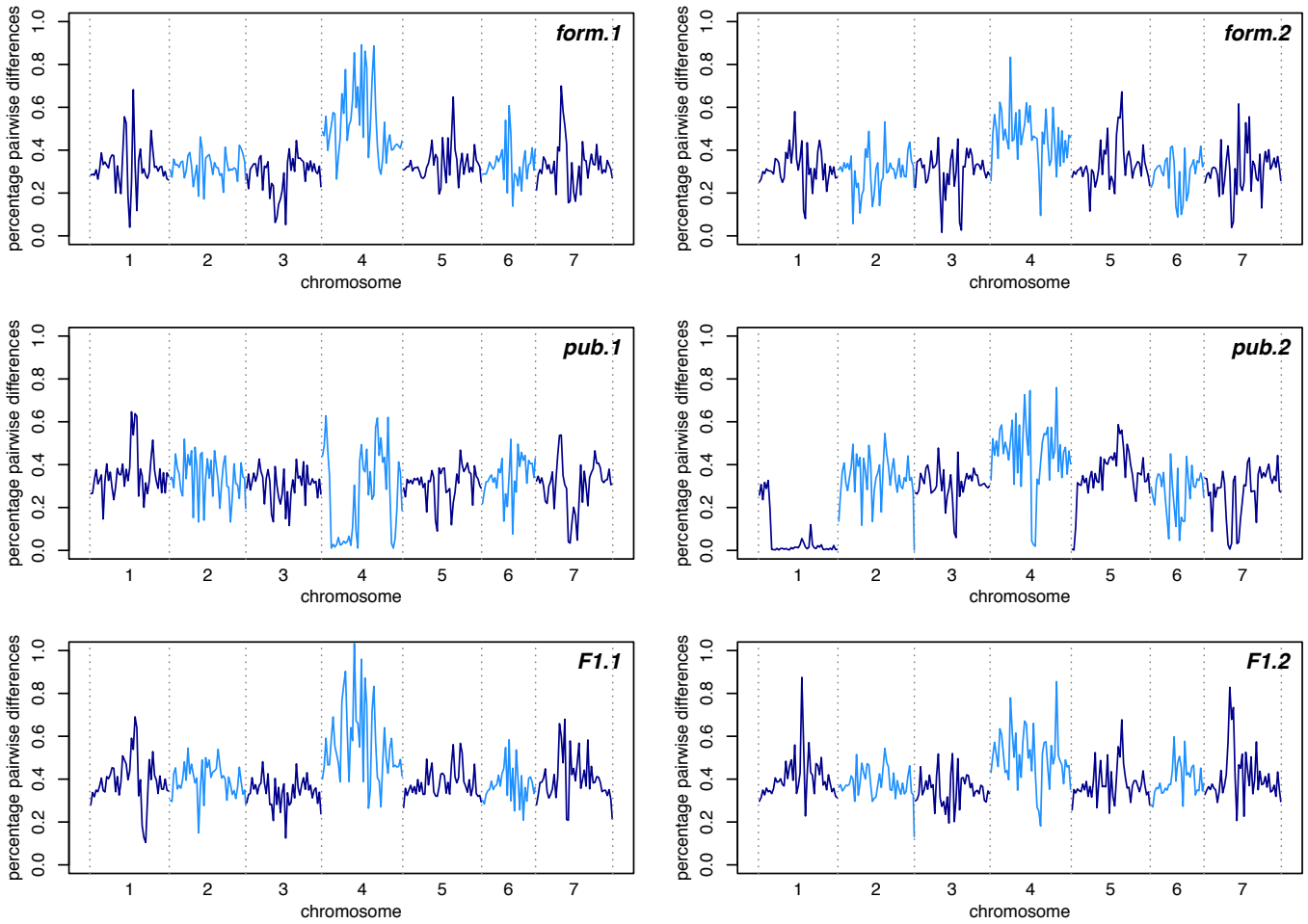

Figure 7-figure supplemental 2. Distribution of gene expression values by chromosome.

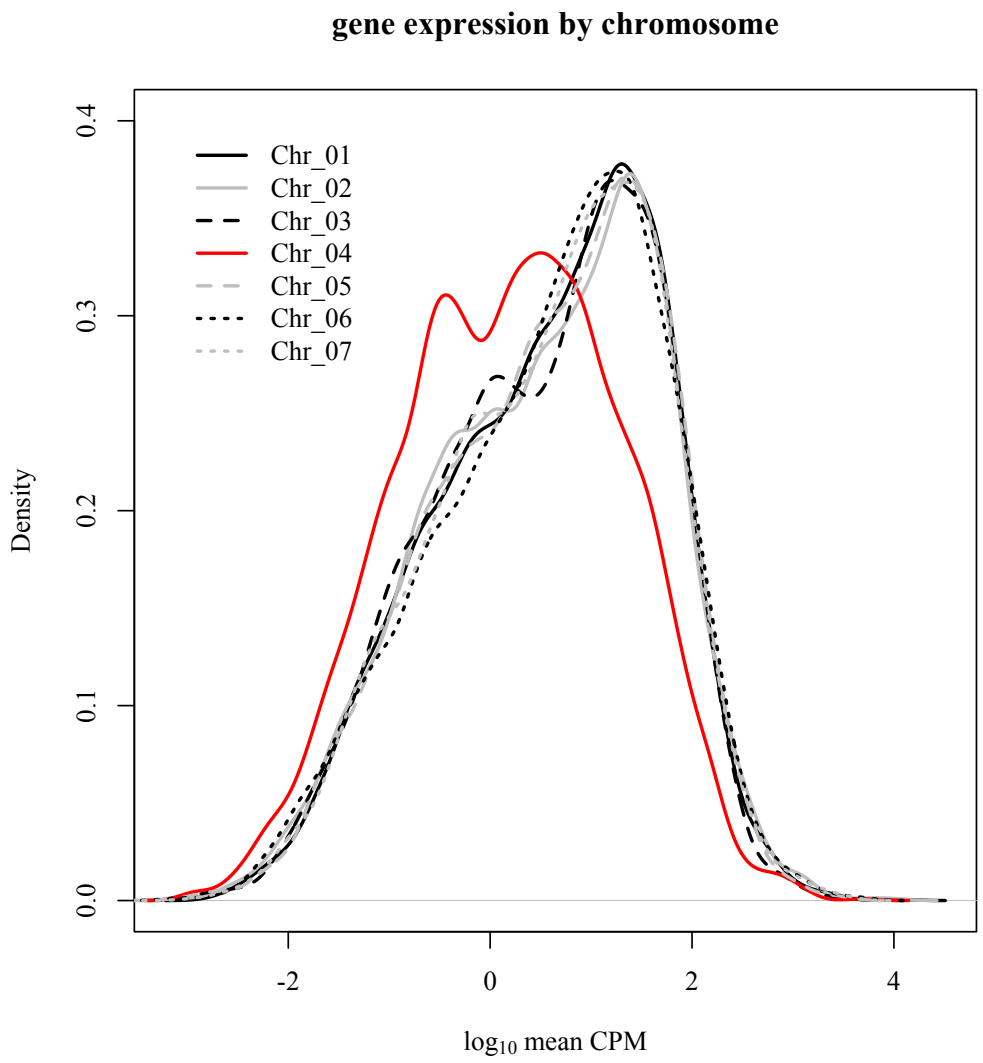

Figure 8-figure supplemental 1. Immunodetection of anti-5mC antibody (pink), and FISH of 35S rDNA (green) and oligoCh4 (red) probes on mitotic and pachytene chromosomes in *Semiaquilegia adoxoides*, *Aquilegia vulgaris* and *A. formosa*. Chromosomes were counterstained with DAPI and inverted using Photoshop CS software (Adobe Systems). Scale bars = 10 μm.

Semiaquilegia adoxoides

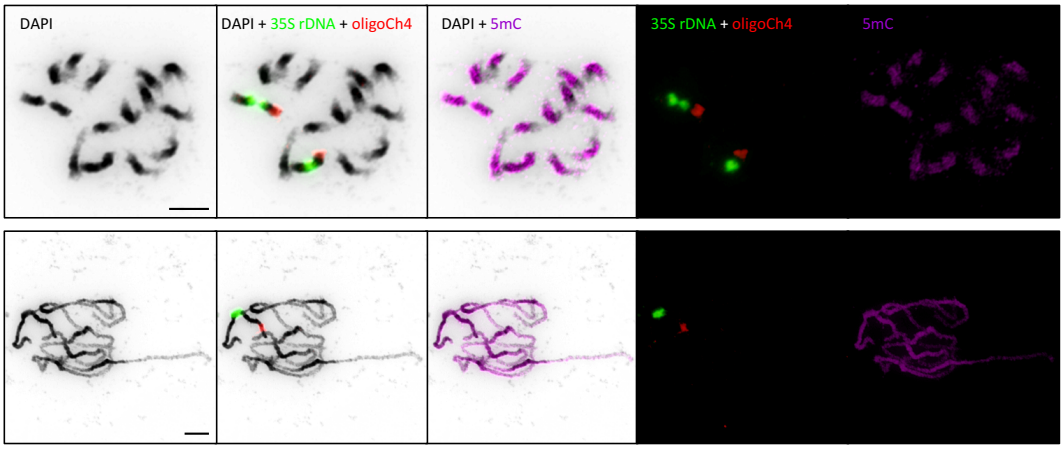

Aquilegia vulgaris

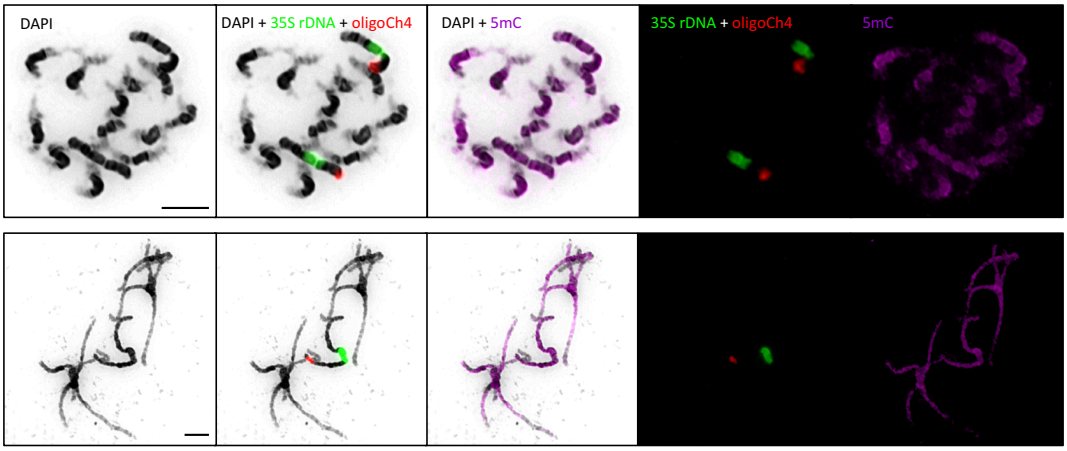

Aquilegia formosa

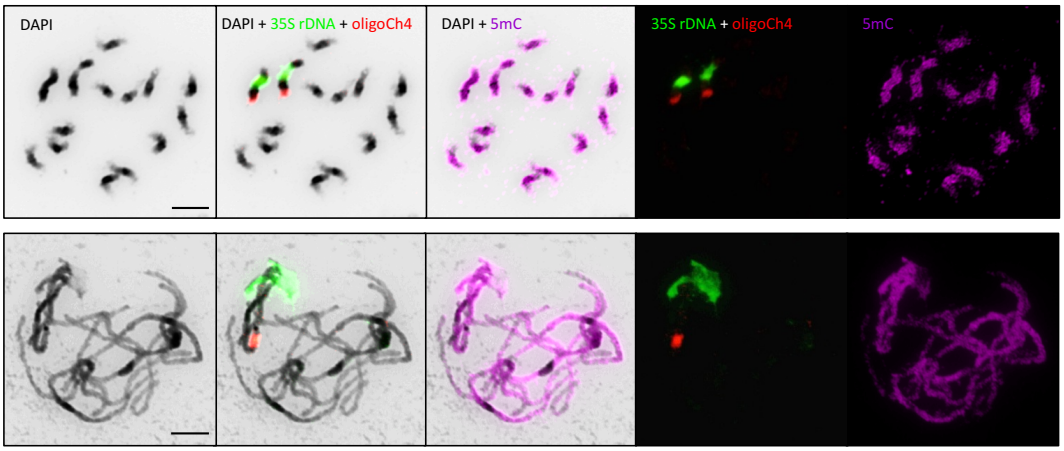

Supplementary File 1. Genomic libraries included in the *A. coerulea* genome assembly and their respective assembled sequence coverage levels in *A. coerulea* v3.1 release.

Library	Sequencing platform	Average read/ insert size	Read number	Assembled equence overage (x)
FTOY	Sanger	2,632 ± 200	1,609,053	2.56
GHCH	Sanger	2,638 ± 201	489,984	0.80
FTOX	Sanger	6,458 ± 677	1,804,031	2.87
GHHF	Sanger	6,460 ± 679	519,264	0.83
FTOW	Sanger	33,419 ± 3,521	219,070	0.31
GGNB	Sanger	33,431 ± 3,496	36,768	0.05
COL	Sanger	123,731 ± 38,119	95,040	0.17
Total			4,773,210	7.59

Supplementary File 2. Summary statistics of the output of the whole genome shotgun assembly prior to screening, removal of organelles and contaminating scaffolds and chromosome-scale pseudomolecule construction. The table shows total contigs and total assembled basepairs for each set of scaffolds greater than the size listed in the left hand column.

Minimum scaffold length	Number of scaffolds	Number of contigs	Scaffold size	Basepairs	% Non-gap basepairs
5 Mb	14	1,438	94,320,677	92,114,319	97.66
2.5 Mb	38	2,890	177,446,204	172,758,974	97.36
1 Mb	87	4,445	257,833,655	250,413,462	97.12
500 Kb	119	5,059	282,450,696	273,716,964	96.91
250 Kb	140	5,324	290,151,377	280,639,834	96.72
100 Kb	168	5,631	294,581,469	283,539,175	96.25
50 Kb	194	5,808	296,290,157	284,968,083	96.18
25 Kb	255	6,094	298,499,112	286,606,915	96.02
10 Kb	606	7,055	303,523,673	291,234,712	95.95
5 Kb	1,202	8,310	307,762,011	295,088,014	95.88
2.5 Kb	2,152	9,914	311,235,474	298,320,877	95.85
1 Kb	2,226	10,013	311,372,308	298,443,577	95.85
0 bp	2,529	10,316	311,527,937	298,599,206	95.85

Supplementary File 3. Final summary assembly statistics for chromosome-scale assembly.

Scaffold total	1,034
Contig total	7,930
Scaffold sequence total	306.5 Mb
Chromosome sequence	282.6 Mb
Contig sequence total	291.7 Mb (4.8% gap)
Scaffold N/L50	4/43.6 Mb
Contig N/L50	797/110.9 Kb

Supplementary File 4. Placement of the individual BAC clones and their contribution to the overall error rate.

Fosmid clone ID	Length	Chromosome	Start	Stop	Discrepant bases
9413	119658	Chr_02	42736342	42855946	0
9446	173129	Chr_02	20577579	20750820	1
9436	124874	Chr_05	34205168	34328207	2
9431	45731	Chr_06	10559008	10602180	1
9449	183288	Chr_01	2756617	2939634	18
9412	166127	Chr_07	17866735	18030762	33
9419	130227	Chr_03	19399302	19529716	28
9437	119406	Chr_01	36503268	36621202	27
9429	131322	Chr_05	15731088	15862409	35
9450	121062	Chr_05	42742789	42865380	36
9428	137275	Chr_01	18470512	18607862	41
9404	107650	Chr_03	32268312	32374757	35
9427	160464	Chr_07	543990	704396	53
9442	130064	Chr_03	30119597	30129597	48
9416	167046	Chr_05	23092053	23258725	69
9409	140373	Chr_07	31933377	32073020	72
9435	117612	Chr_04	44491410	44609808	63
9403	153476	Chr_02	38659429	38811278	98
9441	87456	Chr_04	6547153	6628689	78
9408	165608	Chr_07	30512052	30676049	236
9444	171059	Chr_04	25447280	25613428	363
9447	65772	Chr_06	1652383	1717537	151
9433	145126	Chr_04	38529772	38643947	343
Total	3,063,805				

Supplementary File 5 is RNA seq datasets - separate file

Supplementary File 6. Ratio of polymorphism (poly) or divergence (div) on each chromosome versus genome-wide for each species. Polymorphism is the number of pairwise differences within a species, divergence is the pairwise differences between the species and Semiaquilegia. Both are calculated at fourfold degenerate sites.

Species	Ratio type	Chr_01	Chr_02	Chr_03	Chr_04	Chr_05	Chr_06	Chr_07
A. pubescens	poly	0.310	1.154	1.167	1.774	1.058	1.109	1.112
	div	0.971	0.973	1.004	1.204	0.972	1.014	1.008
A. barnebyi	poly	0.915	0.868	0.979	2.053	0.968	0.958	0.979
	div	0.974	0.973	1.004	1.206	0.972	1.016	1.003
A. aurea	poly	0.956	0.790	0.807	1.601	1.121	1.834	0.450
	div	0.977	0.969	1.006	1.190	0.980	1.010	1.002
A. vulgaris	poly	0.920	1.239	0.693	1.926	0.806	1.025	1.091
	div	0.977	0.971	1.005	1.189	0.982	1.008	1.001
A. sibirica	poly	0.681	0.436	2.489	1.055	1.034	0.317	0.838
	div	0.979	0.970	1.003	1.205	0.979	1.004	1.003
A. formosa	poly	0.958	0.996	1.020	1.641	0.927	0.879	1.003
	div	0.976	0.973	1.004	1.205	0.970	1.012	1.006
A. japonica	poly	0.931	1.031	0.884	1.790	0.984	1.080	0.868
	div	0.977	0.962	1.005	1.204	0.984	1.008	1.002
A. oxysepala	poly	1.627	0.661	0.542	6.182	0.495	0.350	0.424
	div	0.974	0.969	1.001	1.192	0.987	1.007	1.006
A. longissima	poly	1.630	0.649	0.691	2.780	0.872	0.486	0.869
	div	0.974	0.971	1.001	1.205	0.977	1.011	1.005
A. chrysantha	poly	0.936	1.051	0.979	1.776	0.928	0.913	0.946
	div	0.975	0.972	1.002	1.211	0.974	1.015	1.002
mean	poly	0.986	0.887	1.025	2.258	0.919	0.895	0.858
	div	0.975	0.970	1.004	1.201	0.978	1.011	1.004

Supplementary File 7. Robustness of nucleotide diversity patterns to copy number variant detection methods.

		Percent nucleotide diversity							
		Chromosome							
Method	Species	1	2	3	4	5	6	7	Genome
0.15log cov	*A. pubescens*	0.027	0.097	0.092	0.151	0.098	0.092	0.096	0.084
	A. barnebyi	0.053	0.055	0.046	0.086	0.050	0.046	0.047	0.051
	A. aurea	0.009	0.005	0.005	0.001	0.012	0.017	0.001	0.007
	A. vulgaris	0.103	0.120	0.071	0.156	0.087	0.103	0.113	0.101
	A. sibirica	0.018	0.005	0.084	0.033	0.025	0.005	0.017	0.027
	A. formosa	0.123	0.112	0.116	0.165	0.111	0.122	0.112	0.118
	A. japonica	0.144	0.152	0.143	0.247	0.149	0.151	0.144	0.151
	A. oxysepala	0.042	0.005	0.002	0.116	0.002	0.001	0.001	0.015
	A. longissima	0.029	0.007	0.008	0.037	0.010	0.003	0.013	0.014
	A. chrysantha	0.097	0.106	0.088	0.161	0.097	0.087	0.095	0.098
CNV detection	*A. pubescens*	0.094	0.332	0.316	0.446	0.289	0.293	0.290	0.264
	A. barnebyi	0.196	0.195	0.182	0.351	0.201	0.197	0.192	0.198
	A. aurea	0.030	0.025	0.023	0.017	0.025	0.055	0.013	0.027
	A. vulgaris	0.225	0.295	0.132	0.343	0.190	0.241	0.245	0.223
	A. sibirica	0.055	0.020	0.169	0.034	0.091	0.028	0.061	0.072
	A. formosa	0.305	0.316	0.317	0.436	0.301	0.307	0.316	0.314
	A. japonica	0.307	0.305	0.275	0.551	0.309	0.345	0.296	0.312
	A. oxysepala	0.099	0.033	0.027	0.251	0.020	0.015	0.018	0.046
	A. longissima	0.079	0.032	0.026	0.107	0.033	0.022	0.040	0.043
	A. chrysantha	0.306	0.318	0.282	0.421	0.305	0.301	0.305	0.306
Tandem duplicates	*A. pubescens*	0.082	0.340	0.324	0.473	0.322	0.288	0.305	0.282
	A. barnebyi	0.191	0.197	0.191	0.364	0.200	0.176	0.190	0.200
	A. aurea	0.029	0.027	0.024	0.035	0.043	0.046	0.016	0.031
	A. vulgaris	0.214	0.293	0.164	0.403	0.198	0.217	0.238	0.228
	A. sibirica	0.054	0.033	0.184	0.103	0.073	0.030	0.063	0.077
	A. formosa	0.321	0.325	0.320	0.483	0.318	0.309	0.321	0.328
	A. japonica	0.296	0.314	0.287	0.571	0.299	0.317	0.296	0.314
	A. oxysepala	0.102	0.037	0.027	0.319	0.023	0.018	0.022	0.055
	A. longissima	0.079	0.030	0.037	0.137	0.039	0.018	0.041	0.047
	A. chrysantha	0.304	0.329	0.291	0.496	0.302	0.298	0.312	0.315
Allele ratio in reads	*A. pubescens*	0.045	0.201	0.254	0.471	0.321	0.289	0.305	0.241
	A. barnebyi	0.139	0.135	0.155	0.370	0.198	0.179	0.190	0.176
	A. aurea	0.012	0.007	0.012	0.039	0.044	0.047	0.018	0.023
	A. vulgaris	0.162	0.224	0.127	0.408	0.204	0.219	0.241	0.204
	A. sibirica	0.031	0.010	0.153	0.108	0.074	0.030	0.066	0.065
	A. formosa	0.243	0.230	0.273	0.476	0.318	0.308	0.320	0.290
	A. japonica	0.225	0.234	0.247	0.579	0.298	0.320	0.297	0.283
	A. oxysepala	0.066	0.009	0.012	0.329	0.025	0.019	0.024	0.043
	A. longissima	0.057	0.016	0.027	0.139	0.040	0.019	0.041	0.040
	A. chrysantha	0.226	0.232	0.249	0.495	0.303	0.296	0.310	0.279

Supplementary File 8. Repeat family prevalence and permutation results in the *A. coerulea* v3.1 genome release.

Family	Observed copy number on Chr_04	Number of permutations with fewer	Number of permutations with more	Number of permutations with same
DNA CMC-EnSpm	443	1000	0	0
DNA TcMar-Pogo	637	1000	0	0
DNA hAT-Tip100	49	1000	0	0
LINE CRE-II	1109	1000	0	0
LINE L1	2038	1000	0	0
LINE Tad1	90	1000	0	0
LTR	377	1000	0	0
LTR Copia	4341	1000	0	0
LTR Gypsy	4097	1000	0	0
SINE tRNA	1173	1000	0	0
Unknown	28188	1000	0	0
LINE L2	26	994	2	4
LINE R1	52	998	2	0
DNA hAT-Ac	1376	991	9	0
DNA TcMar-Stowaway	29	951	26	23
DNA MuLE-MuDR	301	961	35	4
LTR Caulimovirus	148	945	46	9
Simple repeat	326	935	57	8
DNA Maverick	27	910	64	26
LTR Ngaro	13	864	68	68
Satellite	41	828	130	42
rRNA	42	811	145	44
DNA hAT	41	719	229	52
LTR ERVK	18	665	247	88
LINE RTE-BovB	14	579	305	116
snRNA	12	557	311	132
DNA MULE-MuDR	299	659	323	18
RC Helitron	135	340	624	36
DNA Crypton	11	250	641	109
SINE?	80	259	700	41
DNA PIF-Harbinger	270	135	848	17
DNA TcMar	51	102	863	35
LTR ERV1	63	48	942	10
DNA	16	2	992	6
DNA hAT-Tag1	381	6	993	1
DNA Sola	1	0	996	4
LINE L1-Tx1	4	0	999	1
DNA Dada	0	0	1000	0

Supplementary File 9. K-mer based estimates of genome size and repetitive sequence proportion

Geographic region	Species	Genome size (bp)	Proportion repetitive
North America	*A. pubescens*	327739099	0.473
	A. formosa	320736307	0.442
	A. barnebyi	314243005	0.449
	A. longissima	315526747	0.452
	A. chrysantha	327663698	0.443
Europe	*A. aurea*	301759711	0.443
	A. vulgaris	298726981	0.419
Asia	*A. sibirica*	289831630	0.417
	A. flabellata	284394029	0.402
	A. oxysepala	316478823	0.452

Supplementary File 10. Mean and median coverage by species.

Species	Mean coverage	Median coverage
A. pubescens	58	46
A. barnebyi	105	88
A. aurea	116	97
A. vulgaris	122	93
A. sibirica	112	91
A. formosa	122	100
A. japonica	124	100
A. oxysepala	116	87
A. longissima	116	94
A. chrysantha	116	94
Semiaquilegia adoxoides	74	31

Supplementary File 11. Proportion of sites removed by each filter (sites can have more than one filter) by chromosome - for initial filtration without Semi.

Chr	HCov*	INDEL	JGIREP	MINCOV	MissCall	RepMask	MULTI	Unfiltered
Chr_01	0.096	0.216	0.373	0.447	0.309	0.029	0.002	0.264
Chr_02	0.101	0.212	0.394	0.476	0.311	0.028	0.002	0.227
Chr_03	0.099	0.214	0.375	0.462	0.291	0.029	0.002	0.245
Chr_04	0.076	0.230	0.520	0.702	0.461	0.028	0.003	0.071
Chr_05	0.099	0.215	0.379	0.464	0.301	0.029	0.002	0.250
Chr_06	0.103	0.213	0.377	0.478	0.330	0.030	0.002	0.240
Chr_07	0.110	0.212	0.389	0.486	0.328	0.029	0.002	0.220

*Hcov=coverage less than 0.5x log median coverage or greater than -0.5x log median coverage, INDEL= indel and +/-10bp, JGIREP=repetitive sequence, MINCOV= coverage <15, MissCall=call missing in any species, RepMask=removed by RepeatMasker, MULTI=multiallelic, Unfiltered=site retained in data

Supplementary File 12. Proportion of sites removed by each filter (sites can have more than one filter) by chromosome - for final filtration with *Semiaquilegia*.

Chr	HCov*	INDEL	JGIREP	MINCOV	MissCall	RepMask	MULTI	Unfiltered
Chr_01	0.089	0.272	0.373	0.541	0.391	0.029	0.003	0.205
Chr_02	0.091	0.265	0.394	0.575	0.398	0.028	0.003	0.176
Chr_03	0.090	0.268	0.375	0.559	0.379	0.029	0.003	0.189
Chr_04	0.054	0.270	0.520	0.800	0.572	0.028	0.004	0.049
Chr_05	0.093	0.271	0.379	0.546	0.378	0.029	0.004	0.195
Chr_06	0.094	0.269	0.377	0.561	0.407	0.030	0.003	0.186
Chr_07	0.098	0.265	0.389	0.577	0.413	0.029	0.003	0.170

*Hcov=coverage less than 0.5x log median coverage or greater than -0.5x log median coverage, INDEL= indel and +/-10bp, JGIREP=repetitive sequence, MINCOV= coverage <15, MissCall=call missing in any species, RepMask=removed by RepeatMasker, MULTI=multiallelic, Unfiltered=site retained in data

Supplementary File 13. Number of derived variants by species.

		Number of variants		
Geographic region	Species	Private	Shared	Total
Asia	*A. japonica*	129211	205724	334935
	A. oxysepala	134400	147923	282323
	A. sibirica	99369	176177	275546
Europe	*A. aurea*	107824	176951	284775
	A. vulgaris	139849	189526	329375
North America	*A. barnebyi*	75641	245644	321285
	A. chrysantha	87258	261239	348497
	A. formosa	87823	266604	354427
	A. longissima	66344	232710	299054
	A. pubescens	72661	265713	338374

Supplementary File 14. Transition matrix for the Five-State Markov process. m_1 denotes the probability of an *A. oxysepala* lineage being a migrant, while m_2 denotes the probability of a *A. japonica* lineage being a migrant at a given generation.

	(1,1,1)	(1,2,0)	(1,0,2)	(1,0,1)	(1,1,1)*
(1,1,1)	1-(m_1+m_2)	m_1	m_2	0	0
(1,2,0)	m_2	1-(2*m_2+1/N)	0	1/N	m_2
(1,0,2)	m_1	0	1-(2*m_1+1/N)	1/N	m_1
(1,0,1)	0	0	0	1	0
(1,1,1)*	0	m_1	m_2	0	1-(m_1+m_2)

Supplementary File 15. Transition matrix for the Eight-State Markov process. X=(1-1/N)^{T} and Y=(1-3/N)^{T}

	(1,1,1)	(1,2,0)	(1,0,2)	(1,0,1)	(1,1,1)†	(0,1,1)	(1,1,0)	(1,1,1)*
(1,1,1)	0	0	0	0	X	1-X	0	0
(1,2,0)	0	0	0	(1-Y)/3	Y	(1-Y)/3	(1-Y)/3	0
(1,0,2)	0	0	0	1-X	X	0	0	0
(1,0,1)	0	0	0	1	0	0	0	0
(1,1,1)†	0	0	0	1/N	1-3/N	1/N	1/N	0
(0,1,1)	0	0	0	0	0	1	0	0
(1,1,0)	0	0	0	0	0	0	1	0
(1,1,1)*	0	0	0	0	X	0	1-X	0